

On the Nonsingle-Site Character of Bis(2-Dimethylsilyl-indenyl)zirconium(IV) Dichloride/MAO and Bis(2-Trimethylsilyl-indenyl)zirconium(IV) Dichloride/MAO: Polymerization Characteristics and Mechanistic Implications

Andreas C. Möller,^{*,†,‡,§} Richard Blom,^{*,†} Ole Swang,^{*,†} Andreas Hannisdal,[‡] Erling Rytter,^{*,†,||} Jon A. Støvneng,[§] and Tanja Piel[⊥]

Department of Chemical Engineering, Department of Physics, Norwegian University of Science and Technology (NTNU), N-7491 Trondheim, Norway, Statoil Research Centre, N-7005 Trondheim, Norway, Department of Hydrocarbon Process Chemistry, SINTEF Materials and Chemistry, P. O. Box 124, Blindern, N-0314 Oslo, Norway, Department of Polymer Technology, Helsinki University of Technology, P.O. Box 6100, FIN-02015 HUT, Finland

Received: October 12, 2007; In Final Form: February 15, 2008

Ethene polymerization with bis(2-dimethylsilyl-indenyl)zirconium(IV) dichloride (**1**)/MAO and bis(2-trimethylsilyl-indenyl)zirconium(IV) dichloride (**2**)/MAO and ethene-*co*-1-hexene polymerization with **1**/MAO are presented. The end group analysis of homopolymers reveals a pronounced dependence of the termination rate on temperature changes. In combination with the high molecular weights obtained, these results are in accord with theoretical predictions. Gel permeation chromatography, Fourier transform infrared, and ¹³C NMR analyses of copolymerization products from **1**/MAO as a function of comonomer concentration at two different temperature series denote its tendency to form inhomogeneous polymer blends. Thermal analysis and fractionation results of one such blend indicate an inhomogeneity in the enchainment process and the existence of multiple active sites of differing geometry. These indications are further supported by AMBER force field and density functional theory studies of the catalyst precursors and the active site of **1**/MAO. For this system, δ -agostic interactions for the stabilization of the zirconium cation are favored over β -agostic interactions, which, in contrast to the situation in studies on bis-Cp systems, is a sparsely populated species. The gap in activation enthalpies for β -hydride transfer and elimination is marginalized for these bulky zirconocenes, and conceptually new mechanisms for the isomerization of the vinyl end groups are discussed. Further, unexpected activation of the silicon–hydrogen bond within the ligand framework is observed with an activation enthalpy as low as 14 kcal/mol.

Introduction

The synthetic and catalysis chemistry of zirconocenes has been explored intensively after the discovery of highly active zirconocene dichloride/MAO systems more than two decades ago.¹ Propelled by early success in yielding isotactic polypropene (iPP) from C₂-symmetric zirconocenes, the quest for tailor-made polymer properties and microstructure was predominantly directed to the rigid ligand framework of ansa-metallocenes or C₅-symmetric metallocenes.² These zirconocenes are well characterized as precursors and as the activated single-site catalysts, though polymers with polydispersity indices close to two are liable to sharkskin effects and leave something to be desired from the processing point of view. Mechanistic investigations are not easy although the structures of these catalysts are known. This is indicated by the numerous suggested

amendments to the polymerization mechanisms, which seem to cover any stereo and chain irregularity ever observed.^{1,2}

Interest in the synthesis and catalysis of unbridged and hence rotationally flexible zirconocenes was reanimated by works of Waymouth et al. a few years ago.^{3a–c} It was claimed that a well-tuned system such as bis(2-(phenyl)indenyl)zirconium(IV) dichloride would behave as a dual-site catalyst and provide elastomeric PP (ePP). A number of fundamental problems with the suggested, underlying mechanism of polymerization have been addressed by Busico et al.,⁴ and the dispute is still not settled.^{3f}

A number of groups embarked on explorations directed toward the synthesis and polymerization catalysis of these unbridged, 2-substituted bis(indenyl)zirconocenes.^{5–10a} Interestingly, it appears that very little effort has been made to investigate copolymerizations,^{10b,14,15} and to the best of our knowledge no detailed quantum chemical explorations have been undertaken on zirconocene systems of this size.

Earlier and elsewhere, we have reported inter alia on the synthesis of bis(2-dimethylsilyl-indenyl)zirconium(IV) dichloride (**1**) and bis(2-trimethylsilyl-indenyl)zirconium(IV) dichloride (**2**) and preliminary polymerization studies.^{10a,b} Since then, we have been working further in this direction and wish to give a full account on the data obtained from ethene homopolym-

* To whom correspondence should be addressed. E-mail: Andreas.C.Moeller@borealisgroup.com; ole.swang@sintef.no; err@statoil.com; richard.blom@sintef.no.

[†] SINTEF Materials and Chemistry.

[‡] NTNU, Department of Chemical Engineering.

[§] NTNU, Department of Physics.

^{||} Statoil Research Centre.

[⊥] Helsinki University of Technology.

[‡] Present address: Borealis Polyolefine GmbH, St.Peter-Str. 25, A-4021 Linz, Austria.

erization studies with 1/MAO and 2/MAO and ethene-co-1-hexene polymerization studies with 1/MAO; conceptual quantum chemical considerations with regard to these systems shall also be mentioned.

Experimental Investigation

Ethene Homopolymerizations. The effect of the silyl substituent on the polymerization activities has been investigated earlier and shall not be expanded further at this time.^{10a} For the homopolymerizations, we were interested in the catalyst's response to a change in temperature to investigate possible multisite behavior. The polymerization temperature was varied from 10 to 80 °C, and the polymers were characterized with respect to molecular weight by means of FT-IR and high-temperature gel permeation chromatography (GPC).

The maximum in activity of 1/MAO was observed for 30 °C in our set of experiments (Table 1). It may be argued that the decrease in activity at lower temperatures could be caused by diffusion effects, but we consider this scenario to be unlikely. For 2/MAO, the same statement is valid. An activity decay above a given temperature is known from literature. Though few attempts to investigate this behavior have been published from the catalysis researcher's camp, a recurring rationale is given in decomposition reactions of the zirconocene.¹¹ Waymouth¹² has claimed possible decomposition products to be polymerization active but has failed to provide evidence other than an increase in polydispersity indices. We are not aware of any works providing experimental evidence and could not procure evidence from our studies that decomposition, for example, by moisture, would afford a new polymerization active site. Further, we are not aware of accounts on zirconium-based catalysts or alkyls that would catalyze C–C bond cleavage after termination of the polymerization reaction. A possible explanation for these deactivation processes will be accounted for in the theoretical assessment (vide infra).

The molecular weights decreased with increasing temperature, as it is expected from theory because the termination reactions are subjected to activation barriers. The activation barrier for propagation is usually low if existent at all,²⁸ and an increase in temperature is therefore not expected to affect the overall enchainment rate as strongly as it does the termination rate. In other words, enchainment is governed by a large exponential term, that is, association rate limit of monomer into the coordination sphere (bimolecular process), whereas for termination the exponential term is still growing and association rate of monomer is not relevant (unimolecular process). The convergence in the molecular weights determined by FT-IR and GPC can be explained by consideration of the rate laws for the different termination reactions. The FT-IR technique overestimates the molecular weight if chain transfer to aluminum (CTA), that is, MAO, occurs to a notable degree. GPC results are likely to underestimate the molecular weights for $PDI \gg 2$, as direct determination methods fail. (Application of the Mark–Houwink equation with the fixed constants for α and K is not a reliable solution, as these values are a function of the hydrodynamic volume. The latter one is influenced by the polydispersity index (PDI), leading to an impasse.) Even though the unimolecular β -hydride elimination (BHE) reactions become energetically affordable at higher temperatures, the bimolecular transfer reactions β -hydride transfer to monomer (BHT) and CTA should be much less endothermic. Though an increase in temperature should provide better accessibility of the BHT reaction, a steep increase of double bond terminations is usually not observed. Theoretical studies predict a compensation of the effects of

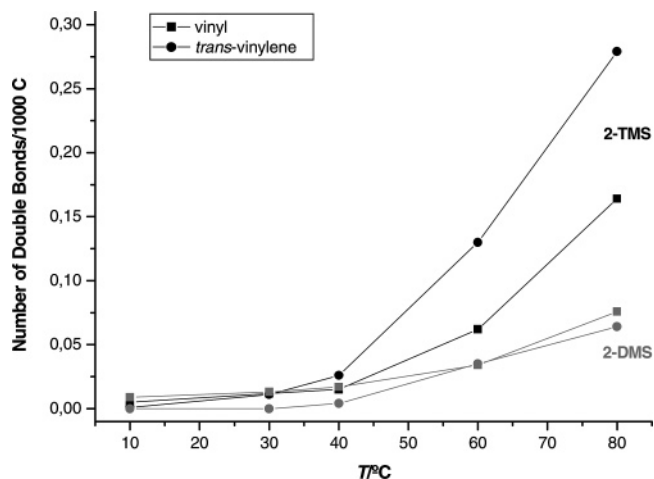
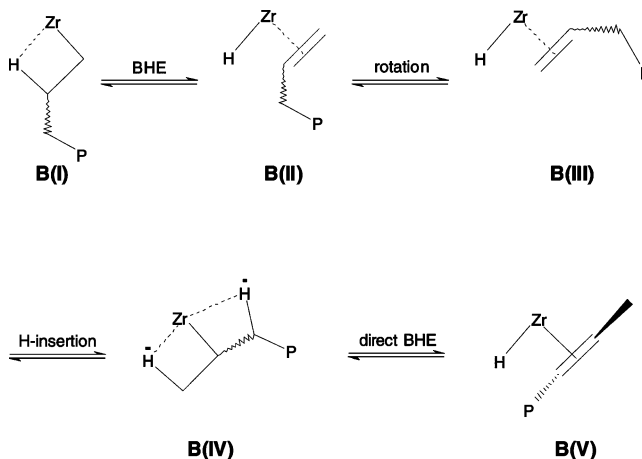


Figure 1. Number of double bonds per 1000 C as found by FT-IR analysis. Dashed line, 1/MAO; solid line, 2/MAO.

SCHEME 1: Classical Mechanism for the Isomerization of β -Agostic Polymer Chain to a *trans*-Vinylene-Terminated Polymer Product^a



^a The mechanism starts from the agostic interaction **B(I)/A(I)**, which will be investigated more closely in the theoretical section and features an unusual double-agostic interaction in **B(IV)**.

increased propagation rate and termination rate.¹³ It must be noted that these studies also predict a closing of the energy gap between the bimolecular and unimolecular processes, as steric congestion at the active site increases.

Quantitative analysis of the double bond terminations reveals opposite situations for 1/MAO and 2/MAO, as illustrated in Figure 1. Vinyl bonds can arise from BHT and BHE, whereas, according to classical mechanistic concepts, *trans*-vinylene double bonds require BHE for subsequent isomerization (Scheme 1). The relative ratio of vinyl to *trans*-vinylene of polymers produced by 1/MAO is, as expected, greater than unity, that is, the main termination route to double bonds has to be BHT or singular BHE. For 2/MAO, a reversal of this ratio is observed, implying a higher rate of BHE for 2/MAO than for 1/MAO. This finding can be interpreted as corollary to the aforementioned predictions suggesting that sterically more encumbered systems would display a higher tendency to BHE, as the activation barrier for a sterically demanding BHT process should increase with steric bulk.¹³ The unimolecular BHE process, in contrast, would be less affected. Simple approaches to an estimate of the relative size of rate constants for propagation and termination reactions are available,^{16a–c} but because of the small number of data points available we did not consider it

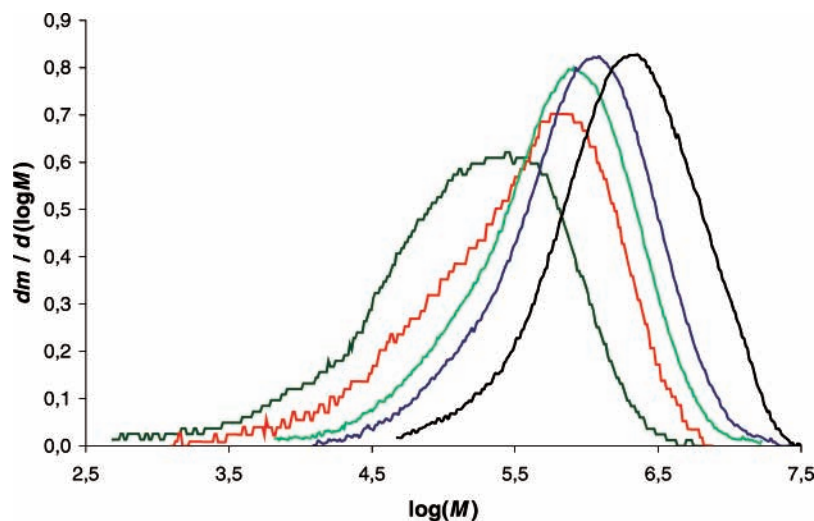


Figure 2. GPC traces for **1b**/MAO in ethene homopolymerizations at $c(E) = 0.14$ mol/L at the temperatures 80, 60, 40, 30, 10 °C (from left to right).

appropriate to follow up such calculations. In addition, these approaches make the assumption that the active sites for propagation and termination are identical as far as ethene is involved. This assumption can be highly disputable for single-site-catalysts^{16d} and appears positively invalid for the catalysts presently under study: Irrespective of the counterion, single-site catalysts display a PDI of two, while the systems **1**/MAO and **2**/MAO display a much higher and temperature-dependent value. Multimodal polymer blends could be identified and fractionated. Therefore, these catalyst are very likely not single-site catalysts in the classical sense.

The polydispersities do increase with temperature, and we suggest that this behavior is not due to decomposition reactions but to the existence of active sites that only become thermodynamically accessible at higher temperatures, for example, different conformers of the several possible active sites. Because of the short lifetimes of the active sites, this claim remains difficult to verify, but a theoretical approach will be presented in the course of this contribution. Circumstantial evidence is given by the shape of the GPC elution curves, which reveal a temperature dependence (Figure 2).^{10b}

Ethene-co-1-hexene Polymerizations. Earlier, we have reported trends in activity of different silyl-functionalized 1- and 2-substituted bis(indenyl)zirconocenes at a 1-hexene mole fraction of $X_H = 0.60$.^{10b} The dependence of the polymer microstructure had been investigated, and we now wish to report on isothermal polymerization with a variation of the comonomer mole fraction in the feed.

The results of the more thoroughly investigated impact of 1-hexene in the feed on the catalyst activity at 30 and 80 °C is illustrated in Figure 3 for **1**/MAO; **2**/MAO displayed too low an activity to allow useful studies of this system. The inhibition of the active site by 1-hexene is evident from the shape of the curves, to which the experimental data is listed in Table 2. The deviation between experimental results was too low to be visibly plotted in the graph. Above a comonomer mole fraction of 95%, significant activity could not be observed. 1-Hexene homopolymerizations carried out for 3 and 10 h did not afford reportable yields of poly(1-hexene). GC/MS analysis of the obtained reaction products gave indication for the presence of small amounts of di- and trimers, but quantitative analysis has not been attempted.

Fundamental analysis of the copolymer composition has been conducted by means of FT-IR and high-temperature GPC (Table

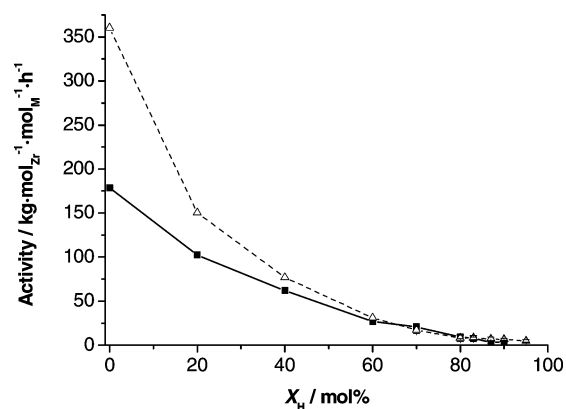


Figure 3. Polymerization activity of **1**/MAO as a function of 1-hexene mole fraction in the reaction feed at 30 °C (triangles, dashed line) and 80 °C (squares, solid line). Conditions: 100–400 mg MAO/100 mL toluene, $c(Zr) = 1.5 \times 10^{-7}$ to 4.0×10^{-6} mol/L.

2). As expected, comonomer incorporation increases with increasing comonomer concentration in the feed and declines with increasing temperature. The molecular weight shows the same trend, though here temperature is more significant than comonomer concentration. Samples obtained at 30 °C and $X_H > 0.6$ were difficult to analyze with respect to end groups; we found a strong dependence of the results on the sample preparation for FT-IR and ¹³C NMR analysis. The latter has been used to validate the reliability of the comonomer content determined by means of FT-IR. The results (which are given in the supporting material) do not show a systematic error and reasonable agreement between both methods is observed, even though two essentially identical NMR samples displayed a deviation by 50%. We assign this behavior to the extremely broad molecular weight distributions of these samples. Discussion of the results obtained focuses therefore on the series at 80 °C.

Melting points and hence crystallinity could be observed for all samples obtained. Flory described the melting point depression of a polymer in the presence of a solvent by modifying equilibrium thermodynamic's standard expression for the solubility of a crystallizable solid in a noncrystallizable "solvent" (eq 1).^{17a} This is essentially the standard equation for the description of the solubility of a solute, as it can be found in any textbook on physical chemistry, applied to the depression of a melting point. In Flory's case, an interaction parameter χ

has to be defined, while Waymouth et al. substituted p by the mole fraction of comonomer incorporated.¹² We have assumed the heat of fusion for crystalline polyethene segments to be 0.960 kcal/mol.^{17b} Accounting for the melting point of the ethene homopolymer as the standard melting point T_m^0 , p will resemble the mole fraction of crystallizing chain segments, that is, x_E or $1 - x_H$ ¹²

$$\frac{1}{T} - \frac{1}{T^0} = \frac{-R}{\Delta H_f} \cdot \ln p \quad (1)$$

This relationship can clearly only be valid if the parameter p describes a stationary system of homogeneous composition, that is, if the comonomer displays colligative character. The term homogeneous is in this context restricted to the macroscopic behavior of the polymer chains; even stationary but inhomogeneous systems with comonomer-enriched chain segments or block copolymers could be described by this equation if the slope and definition of the parameter p is chosen carefully. The graphical representation of the predicted and measured melting points is given in Figure 4 and shows significant deviations between experimental and predicted melting points, though the large error margins provide a reasonably good agreement for high comonomer concentrations. Though the slopes of the two curves are in good agreement, we have to conclude that the parameter p is not related to the comonomer mole fraction in the suggested way. Hence, the copolymers investigated here do not show a homogeneous composition arising from a stationary polymerization process.

The observed GPC elution curves support this claim. The series at 30 °C proved rather difficult to analyze. We did, however, find bimodal product distributions as the one depicted in Figure 5. Results on the presumably multimodal products of the series at 80 °C have been reported elsewhere.^{10b} Exhaustive Soxhlet extraction of the bimodal polymer sample, which was obtained at 30 °C and $X_H = 0.80$ and presented in the aforementioned paper with the solvents diethyl ether, *n*-pentane, *n*-hexane, *n*-heptane, cyclohexane, and toluene afforded six fractions. Differences in morphology were apparent already on visual inspection, although GPC analysis revealed rather pure separation only for the diethyl ether and cyclohexane fraction (Figure 6). All fractions display PDI around 2. The ¹³C NMR and GPC analysis data of these fractions are listed in Table 3. It is evident that the copolymerization products are blends and that the comonomer distribution in these copolymers is inhomogeneous and likely to originate in a nonstationary process, as indicated by the results obtained by thermal and end group analyses. The insufficient separation of the blend by the employed extraction technique may be ascribed to a possible inhomogeneous distribution of the comonomer along the chain. If a comonomer-enriched chain segment is in principle not crystallizable while another segment cocrystallises with highly crystalline polymer, the extraction will be precluded by the solubility difference of amorphous and crystalline assemblies.

Theoretical Investigation

Zirconocene Dichlorides. The potential energy surface as a function of the two improper angles φ and ϕ , that is, Si(a)–C2(a)–C2(b)–Si(b) and Si(a)–C2(a)–Zr–Cl1, respectively, of a zirconocene dichloride may be considered a suitable means to assess effects imposed by changes in the ligand framework (Figure 7). Because the huge number of possible conformers and the two degrees of freedom considered, the use of inexpensive molecular mechanics calculations is the only way

TABLE 1: Catalyst Activity and Molecular Weights of 1/MAO and 2/MAO in Ethene Homopolymerizations at $c(E) = 0.14$ mol/L, that is, 1.2 Bar at 30 °C, 200 mL Toluene

catalyst	$T/^\circ\text{C}$	activity/kg mol _{Zr} ⁻¹ h ⁻¹	$M_n/10^3\text{g mol}^{-1}$			
			Al/Zr	FT-IR	GPC	PDI
1/MAO	10	702 900 ^a	17400	1528	698	3.6
	30	786 100	17400	1045	331	3.7
	40	655 100	17400	688	218	5.2
	60	476 500	17400	203	103	5.7
	80	490 900	17400	100	25	13
	60	1 184 300 ^b	9500	n.d. ^c	n.d.	
	80	1 147 100 ^b	9500	n.d.	n.d.	
	10	112400 ^a		2176	373	3.2
	30	161700		614	242	3.3
	2/MAO	40	98900	3500	340	124
	60	46900		73	45	5.9
	80	9900		32	4.1	7.5

^a Because of experimental difficulties, we assume a concentration of 0.17 mol/L for the experiments at 10 °C. ^b Repetition experiments at these temperatures were carried out on a different reactor; key differences in conditions: 100 mL toluene, 50 mg MAO/100 mL toluene. ^c Not determined.

to obtain something even close to a complete conformational analysis of the systems. This approach has been reported earlier by other groups,^{19,20} and we considered the parameter set used by Brinztinger et al. appropriate for our problem.

Figure 8 and 9 show the molecular mechanics potential energy surfaces for **1** and **2** without consideration of solvent effects. An isomerization path analysis has only been conducted for **1** and the result is outlined in Figure 10. The activation enthalpies for the several isomerization steps are estimated to 3–4 kcal/mol. The most favorable A–A' isomerization paths are A–E–F–B'–A' and A–C'–B'–A', that is, front-side and back-side passage of the two silyl groups, respectively. Conformer A is somewhat rac-like, with its silyl substituents pointing away from the chlorides. Isomerization toward a meso-like form proceeds via E (rac-like), D or F (both silyl groups perpendicular to each other, one between the chlorides) to C or B' (both are synclinal meso-like conformers). Note that all stationary points indicated here are energetically accessible at ambient temperature.

Because of the higher degree of symmetry of the trimethyl silyl (TMS) compared to the dimethyl silyl (DMS) group, the evaluation of the quality of the calculated potential energy surfaces was conducted on **2**. Sixteen arbitrarily chosen conformers of **2** were subjected to density functional theory (DFT) single point calculations at the B3LYP (6-31G* and 6-311G**) levels of theory. Further, three MP2/6-31G* energies were computed. Comparing the MM and DFT single point calculations over 15 arbitrarily chosen energy differences within each series, we found mean deviations of $-2.1 (\pm 2.5)$ kcal/mol_(6-31G*) and $-1.55 (\pm 2.7)$ kcal/mol_(6-311G**). The deviation between the two basis sets showed a mean value of $-0.5 (\pm 0.8)$ kcal/mol. Comparison of the B3LYP energies with the three MP2 energies delivered mean deviations of 0.3 (± 1.1) and 0.1 (± 0.3) kcal/mol, depending on the basis set. It may be concluded that the AMBER force field slightly but consistently underestimates the transition state energies with a rather high standard deviation, while excellent agreement is found among the three quantum chemical approaches.

Despite the promising results obtained from a statistical analysis of agreement between force field and DFT energy differences, we found severe deviations between these methods regarding the structures reported in Figure 10. The agreement for the meso-like conformers is qualitatively very good, but the

TABLE 2: Results for FT-IR and High-Temperature GPC Analysis of LLDPE-Polymers as a Function of 1-Hexene in the Reaction Feed at 80 and 30 °C

X_H / mol %	$x_{H,FTIR}$ / mol %	M_n / $10^3 \text{ g}\cdot\text{mol}^{-1}$	PDI	T_m^a / °C	X_C / %
$T = 80 \text{ °C}$					
0	0.0	43	5.9	136.7	76.6
20	0.9	15	16	127.5	68.4
40	2.0	10	12	124.9	59.9
60	2.5	9.1	8.1	123.0	59.2
70	3.5	7.0	4.1	119.9/111	51.5
80 ^b	5.0	7.5 (± 0.7)	5.0 (± 0.6)	118.9/108/72	48.0
83 ^b	5.7	4.8 (± 0.6)	6.1 (± 0.6)	119.2/103/72	43.7
87 ^b	5.4	3.6 (± 0.7)	5.8 (± 1.3)	119.5/103	38.5
90 ^{b,c}	6.7	6.1 (± 1.3)	3.5 (± 0.8)	115.5/101	45.6
$T = 30 \text{ °C}$					
0	0	342	3.6	136.2	62.7
20	1.0	136	5.7	120.0	42.2
40	2.5	104	8.5	121.4	41.3
60	5.1	85	7.0	114.7/90	22.4
70 ^b	10.2 (± 1.0)	12 /13	43/9.8	108.9/74	2.7
80 ^b	12.1 (± 0.1)	8.6/3.7	38/107	103.5/64	3.2
83 ^b	13.4 (± 0.5)	12/7.8	29/33	102.5	2.8
87 ^b	13.2 (± 0.3)	10/5.6	32/58	98.0	3.0
90 ^b	15.3 (± 1.0)	12/9.4	34/35	97.4	2.9
95 ^b	20.5 (± 4.6)	12/14	24/15	91.2	2.2

^a Polymer melting points are reported for one sample only. All values reported in case of multiple melting points. ^bThree independent polymerization experiments were run at 80 °C, two at 30 °C. Average analysis value averaged over experiments. ^c ¹³C NMR analysis suggested an incorporation of 3.0 and 5.0 mol % for these two experiments, qualitatively resembling the same trend found by FT-IR with 5.7 and 7.7 mol %.

TABLE 3: Molecular Weights and Polydispersity Indices for a Bimodal LLDPE Copolymer and the Individual Results for the Several Fractions Obtained by Soxhlet Extraction (¹³C NMR Analyses Were Conducted on the Blend and Fractions One and Five)

sample	M_n / $10^3 \text{ g}\cdot\text{mol}^{-1}$	PDI	x_H /mol %	triads ^a					
				EEE	EEH	HEH	EHE	EHH	HHH
blend	3.7	107	13	0.671	0.179	0.019	0.089	0.039	0.004
F1	26.2/1.3	~2	26	0.440	0.255	0.046	0.167	0.013	0.078
F2	139.9/1.3	~2							
F3	169.2	2.2							
F4	161.3	2.2							
F5	192.3	2.2	10	0.744	0.147	0.008	0.064	0.034	0.002

^a The sum over all triad probability equals unity for all analyses. Sequence length numbers for ethene and 1-hexene are equal in all cases; the boundary conditions $2\cdot p(\text{EHE}) = p(\text{EEH})$ and $2\cdot p(\text{HEH}) = p(\text{EHH})$ are met. Calculation of the triad probabilities was conducted according to ref 36.

transition states found by force field calculations between the stationary points **D**, **E**, and **F** appear incorrect. Judging by the shape of the curve, a minimum may be expected between the two transition states in that aforementioned series and the force field minimum **E** is possibly a transition state on the path to **A**. The problem identified here is in agreement with the large experimental standard deviation found in the statistical analysis of the relative energy differences obtained from DFT and MP2 single point calculations compared to MM single point energies.

Agostic Interactions of the Polymer Chain. In a series of publications, Ziegler et al. tried to validate and unify the several mechanisms suggested by experimentalists in the field of zirconocene catalysis.^{22a-d} A bis(η^5 -cyclopentadienyl)zirconium complex with one ethene and ethyl ligand served as the model for the active site of the polymerization. The β -agostic interaction turned out to be the most stable for that particular catalyst system, and it was assumed that the γ -agostic interaction after the insertion of the olefin would be interconverted to a β -agostic prior to the next olefin association. Thiel et al. explored unusual chain branching phenomena in the polymerization of norbornene.²³ Theoretical and experimental findings indicated the existence of higher agostic interactions, that is, beyond α and β , and their leading to isomerization by means of a σ -bond metathesis reaction.

For the cationic bis(2-DMS-ind)zirconium system's agostic interaction with the polymer chain we have found the fully DFT-optimized energy profile depicted in Figure 12. A simplified illustration and the assignment of the acronyms of the different geometries is given in Figure 11. The polymer chain model (2-methyl hexyl) resembles a short polymer chain with a branching point after propene enchainment, which we considered a suitable compromise model for a higher α -olefin with regard to computer resources. Geometries **A(I)** and **A(II)** (β - and γ -agostic, respectively) are obviously of similar stability, deviating from each other by only 0.3 kcal/mol and being separated by an activation enthalpy of 3.5 kcal/mol. Although the interconversion from the insertion product **A(II)** to **A(I)** was expected to proceed easily, the equilibrium of these two geometries is surprisingly balanced. In contrast to the findings of Ziegler et al.,^{22a-d} the δ -agostic interaction **A(III)** is significantly more stable than any other calculated geometry. Accounting for the low activation enthalpy calculated for the transition from **A(I)** to **A(III)** and a slow chain propagation reaction, the steady-state concentration of **A(II)** and **A(I)** will be lower than that of the most stable species **A(III)**. At high propagation rates, the geometries **A(I)** and **A(III)** are likely to be sparsely populated and **A(II)** would be a suitable model for the active site. The ϵ -agostic interaction is clearly less stable, and the transition states leading to this

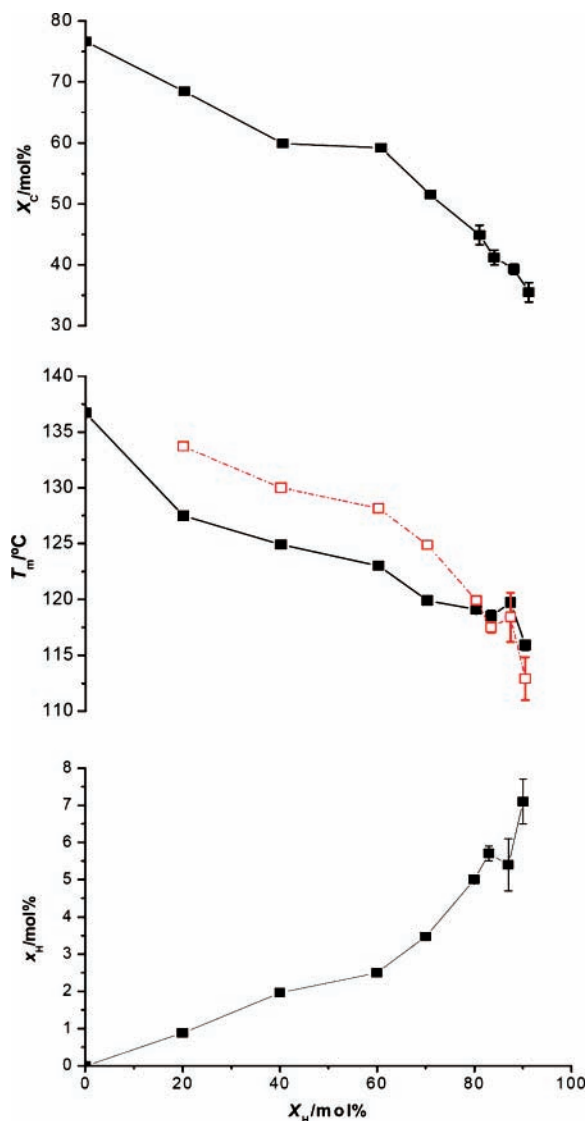


Figure 4. From top to bottom; crystallinity X_c , melting point T_m , and 1-hexene incorporation x_H as a function of the comonomer mole fraction X_H in the polymerization feed for 1/MAO at 80 °C. Experimental values are printed solid and black, theoretical values are dashed.

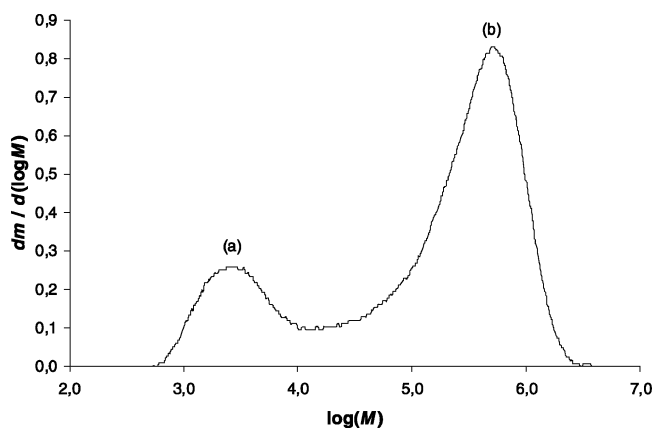


Figure 5. Example for a bimodal product as found in the copolymerization series at 30 °C for 1/MAO at $X_H = 0.80$.

geometry have not been calculated. It may be speculated that **A(IV)** could represent a stationary point in the transition **A(II)-A(III)**. Since the activation energies for the transitions **A(III)-A(I)** and **A(II)-A(III)** are identical within significance, **A(I)** has most likely the shortest lifetime and the lowest population

density. This would explain the observation of high molecular weight polymers for sterically demanding systems, as a BHT termination process commencing from a sparsely populated **A(I)** is not likely to occur.

Scherer and McGrady have recently published a detailed study on the existence of different agostic interactions.²¹ It claimed that the interaction would be favored by hyperconjugation of electron density from the metal-carbon bond along the alkyl ligand. A prerequisite for hyperconjugation to occur is a resonance integral significantly different from zero; indeed the β -agostic chain is frozen in a conformation yielding large resonance integrals. For the more stable γ - and δ -agostic interactions, however, the orbital overlap is minimized, and hence our results indicate that hyperconjugation is not an important factor in the formation of agostic interactions.

Adopting Ziegler's popular argument that the most stable species in the catalytic cycle is the precursor to olefin enchainment,^{22a} we have to conclude that **A(I)** is not a predominant species in our system. Nevertheless, we cannot preclude that a species of rather high energy dominates in chain propagation and refer to other works in the field of catalysis, where such a situation has been observed.^{24a-c} Recent works by Bochmann et al.^{24d} and Landis et al.^{24e} have instructively illustrated the complications connected to the mechanistic studies of metallocene catalysis. While the former reported on possible nonsteady-state conditions during the polymerization and counterion effects on the lifetime of active site species, the latter reported on the erroneous assessment of dormant and active sites.

The catalyst systems 1/MAO and 2/MAO displayed a high degree of end group isomerization in the ethene homopolymerizations. Both systems are sterically demanding, and the active site is encumbered by the ligands. The zipper reaction, as imagined by classical elementary reactions of coordination chemistry, and the isomerization of agostic interactions have been investigated earlier in our group.²⁵ The activation enthalpies reported herein are in good agreement with earlier results. We wish to point out that the first step of the isomerization, which is the shifting of the double bond one carbon atom down the chain, will invoke a sequence of five elementary transformations and will take its starting point in the sparsely populated β -agostic geometry **A(I)**. The increase in steric congestion at the active site and the increase in space required for a BHT render this route unlikely. Additionally, all our attempts to find a stable (olefin) zirconium hydride species failed and resulted in β -agostic alkyl complexes. For sequential BHE reactions, this implies that chain initiation by ethene insertion is more probable than reinsertion of the polymer chain, vide ultra. Bearing in mind that BHT is generally more favorable than BHE, a direct transfer of hydrogen from a stable intermediate emerges as a compelling hypothesis. One such reaction, as shown in Scheme 1, would require three elementary steps neither of which include the rotation of olefin ligands.

The Fate of β -Hydride Elimination Products. BHE has been investigated earlier by other groups and it is generally consented that the activation barrier is rather high at 30–40 kcal/mol.^{26,27} BHE is therefore not a predominant process at low temperatures and BHT and chain transfer to aluminum (CTA) are more likely to occur as long as the steric constraints of the ligand framework do not suppress a bimolecular termination reaction.²⁸ We have reported earlier on the experimental determination of the activation energy for termination processes leading to vinylidene terminations.^{10b} In the following, we shall address the different reaction products and transition states on

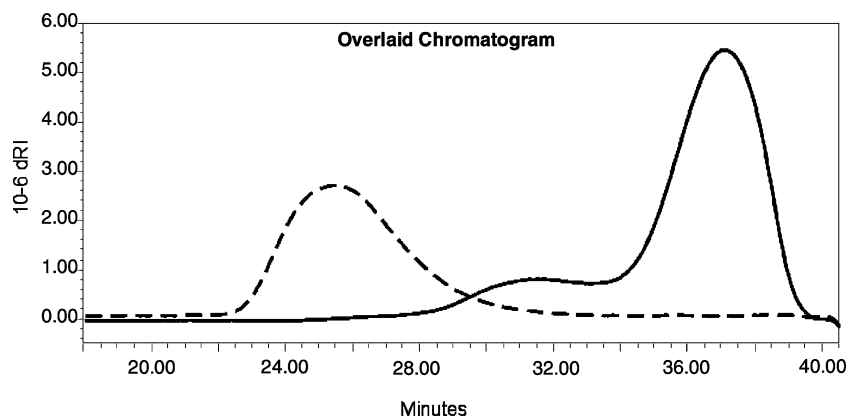


Figure 6. Overlaid GPC chromatogram of fractions 1 and 5 of the extracted polymer blend. Polymers of higher molecular weight will be eluted earlier (Figure 5, left peak), while lower molecular weight fractions remain longer on the column (Figure 1, right peaks). All three peaks display a PDI of ~ 2 .

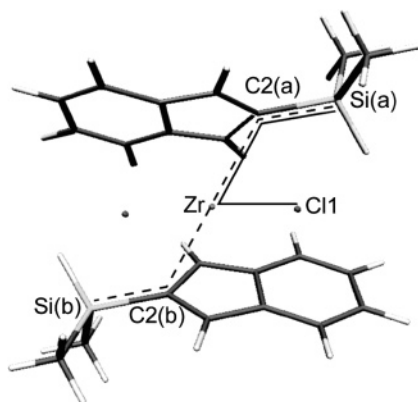


Figure 7. Definition of the angles φ and ϕ , that is, Si(a)–C2(a)–C2(b)–Si(b) (dashed line) and Si(a)–C2(a)–Zr–Cl1 (solid line), in the rac-like conformer of **1**.

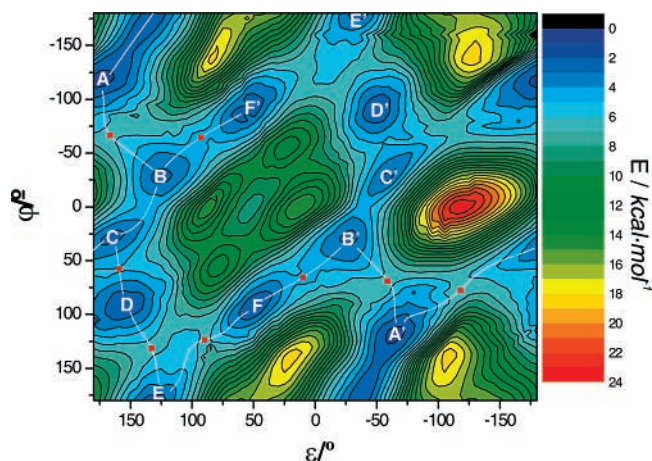


Figure 8. Potential energy surface of bis(2-DMS-ind)zirconium(IV) dichloride as a function of the improper angles φ and ϕ . The energy scale is plotted from 0 to 24 kcal/mol. Local minima are indexed by letters, enantiomers denoted with primes, and transition states marked as red squares.

the basis of quantum chemical results to obtain a more thorough understanding of the impact of the bulky ligand framework compared to the typical Cp-based model systems.

Computational investigation of the simplest BHE reaction with an ethene–hydride complex failed to provide a local minimum representing an ethene π -complex. As starting geometries, zirconium–hydride distances between 1.72 and 2.10 Å were applied²⁹ to no avail. The hydride–zirconium–carbon angle was at least 85°, but even geometries with restrained

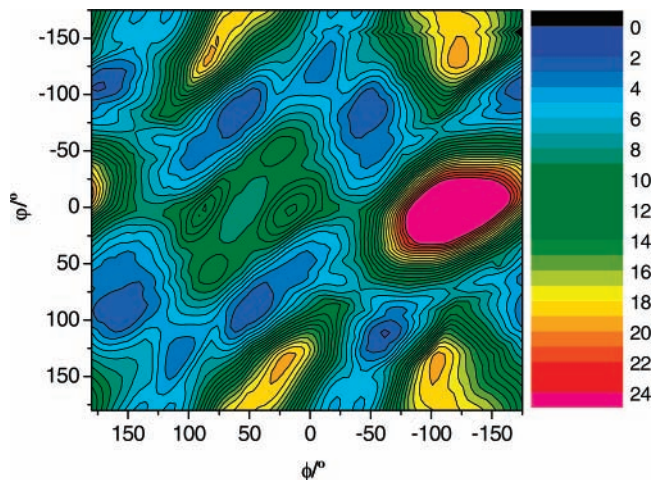


Figure 9. Potential energy surface of bis(2-TMS-ind)zirconium(IV) dichloride as a function of the improper angles φ and ϕ . The energy is given in kcal/mol.

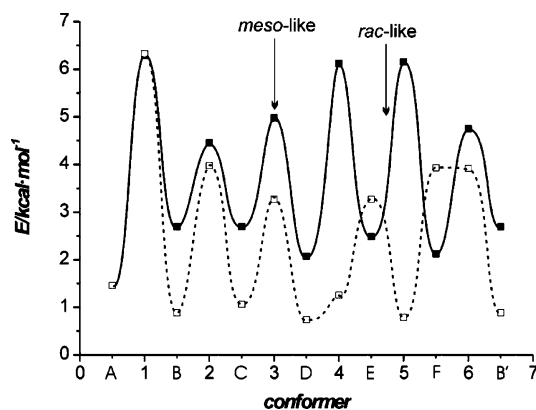


Figure 10. Schematic potential energy diagram for the interconversion of the different conformers along the path shown in Figure 9. The conversion from A' to C is not included in this plot; its transition state energy is estimated to 6.2 kcal/mol. Solid line: AMBER. Dashed line: B3LYP/6-311G**. The DFT single point energy of conformer A has been arbitrarily chosen as a reference point for both traces in this illustration.

H–Zr–C_{olefin} angles would finally add the hydride to the olefin and form a β -agostic ethyl complex upon unconstrained relaxation. Ultimately, with an ethene unit placed 3.89_{C(1)} and 3.99_{C(2)} Å away from the zirconium center, that is, at the outer limit of the coordination sphere, association occurred readily and insertion of the hydride was observed. These results render

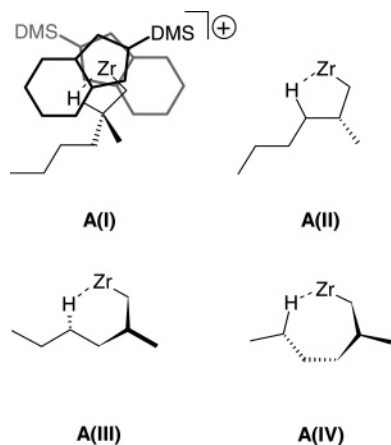


Figure 11. Schematic illustration of the β , γ , δ , and ϵ -agostic interactions, that is, **A(I)**, **A(II)**, **A(III)**, and **A(IV)**, respectively. The silyl substituents on the indenyl ligands point backward; the conformational angle and corresponding energy of the stationary point are given in Figure 12. For clarity, charges and ligands have been omitted for all but **A(I)**.

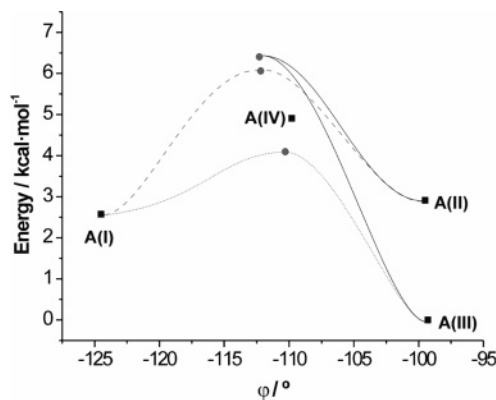


Figure 12. Energy profile from DFT calculations in kcal/mol for the interconversion of β , γ , δ , and ϵ -agostic interactions of the polymer chain and their conformation coordinate φ in degrees. Stationary points (local energy minima) are represented by squares, whereas transition states are represented by gray circles. The constitution of **A(I)–(IV)** is given in Figure 11. The lowest energy computed, that is, **A(III)**,²¹ arbitrarily has been set to zero kcal/mol.

the zirconium-hydride species an active site in the polymerization process, which contradicts the experimental investigation of model systems by Bercaw et al. and Jordan et al.¹⁸ We assign this discrepancy to the presence of strong donor ligands (phosphines, nitriles), the lower oxidation state and high steric congestion of the bisCp* scandocene or, in the case of the zirconocene, the vicinal hydrido and alkyl ligands in the cited works.

To account for the reactions in the course of copolymerizations, different chain termination mechanisms must be considered. For the substituted α -olefins 1-nonene, 2-propyl-1-hexene, and *E*-4-nonene, serving as models for vinyl, vinylidene, and *trans*-vinylene terminations, respectively, the sterically demanding alkyl groups are oriented toward the center of the catalytic site and intrude into the space between the hydride and the olefin. As a result, the olefin is distorted from the ideal coordination observed for ethene. In the case of the rather symmetrical *E*-4-nonene, the distances for C(1) and C(2) to Zr measure 2.64 and 2.96 Å, while the *E* constitution requires a tilting of the double bond around the Zr-olefin axis. The tilt angle, defined as H–Zr–DC–C2 with DC denoting the midpoint between C(4) and C(5) of the olefin, is as large as -42.9° for the internal *E*-4-nonene. For the terminal 1-nonene,

TABLE 4: Transition State Energies for the Three Different BHE Terminations Possible in Ethene-*co*-1-hexene Polymerization and the Stabilities of the Several Products Relative to the TS (for Each Termination, the Unbranched Polymer Chain before Elimination Arbitrarily Has Been Set to Zero kcal/mol as a Reference Point)

Termination	Transition State (kcal·mol ⁻¹)	Product Stabilisation (kcal·mol ⁻¹)	Product (kcal·mol ⁻¹)
	17	-1	16
	14	-6	8
	16	-1	15
	16	± 0	16

^a Because of the double-agostic interaction in the starting geometry of the BHE reaction step forming a *trans*-vinylene termination, it is in principle possible to form a vinyl termination. This is indistinguishable from an ordinary vinyl termination but follows a separate reaction trajectory.

the tilt angle of the double bond is much smaller, as one side of the olefin is hydrogen-terminated and sterics allow a deeper intrusion of this unsubstituted side into the ligand sphere of Zr, affording hereby a stronger coordination of the olefin. The angle measures -24.1° and the Zr–C(1) distances shorten to 2.63 Å, whereas the Zr–C(2) distance grows to 3.00 Å. Apart from the tilt angle, the two stationary points for the internal and the terminal olefins are fairly alike. More pronounced, but still following the trend, the coordination of 2-(1-propyl)-1-hexene is described by a tilt angle of 2° and the distances of 2.62 and 3.24 Å for the zirconium carbon distances.

Energetic comparison of the several olefin complexes requires the stoichiometry to be constant. During searches for the more labile transition states, the long paraffin chains have, however, a detrimental effect on geometry optimization convergence because of the introduction of numerous “soft modes”, that is, molecular deformations requiring very little energy. Therefore, the transition states for the formation of vinyl, vinylidene, and *trans*-vinylene terminations had to be calculated with the smallest realistic polymer model. The obtained transition state energies are not directly comparable due to differences in stoichiometry, but note that the relative energy difference obtained from the relaxation products of slightly perturbed transition states affords the correct activation enthalpy for the matter of subject. The results for the several reactions are summarized in Table 4.

Vinyl terminations obtained from a 1-butyl polymer chain (**E(I)**) proceed via a transition state with an imaginary vibrational mode at 361i cm⁻¹. The corresponding activation enthalpy of transition state **ETS 1** is calculated to 17 kcal/mol, whereas the hydride-olefin complex **E(II)** is only stabilized by a marginal 1 kcal/mol (cf. Figure 13). The subsequent rotation of **E(II)**'s olefin around the imaginary Zr-olefin axis proceeds via two transition states of which **ETS 2** has been estimated to be destabilised by 2 kcal/mol with respect to **E(II)**. Naturally, the two transition states are distinguished by one local minimum, which will be considered in the forthcoming paragraph. Relative to the reactant olefin complex **E(II)**, product olefin complex **E(III)** is energetically disfavored and reacts spontaneously, virtually without any activation barrier (**ETS 3**) to the saturated polymer chain **E(IV)** that displays two distinct β -agostic interactions with C–H distances of 1.188 and 1.196 Å,

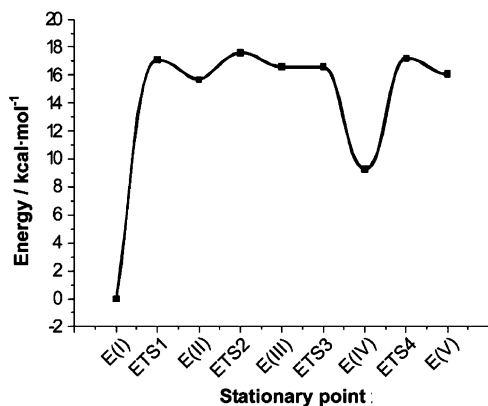


Figure 13. Potential energy diagram for the isomerization of an unbranched polymer chain to a *trans*-vinylene chain termination. The several local minima **E(I)**–**E(IV)** are depicted in Scheme 1 as the minima **B(I)**–**B(IV)**. The lowest energy computed, that is, **E(I)**, arbitrarily has been set to zero kcal/mol.

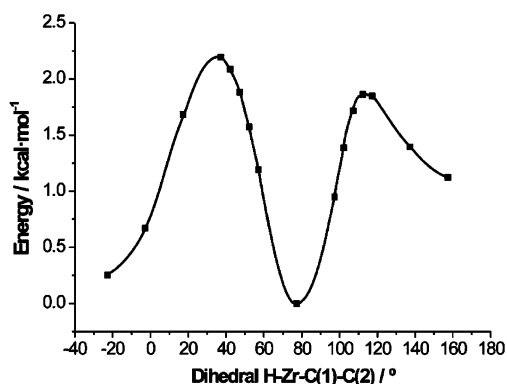


Figure 14. Potential energy curve for the rotation of an α -olefin in the coordination sphere of the zirconium complex. The initial BHE product features a dihedral angle of -22.8° , whereas the rotated olefin has a stationary point at 159.1° . The lowest energy computed arbitrarily has been set to zero kcal/mol.

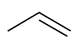
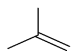
respectively. The final ascent to the 8 kcal/mol higher transition state **ETS 4** affords the isomerization end product **E(V)** featuring the *trans*-vinylene chain termination. This isomerization product is 16 kcal/mol less stable than the unbranched polymer chain.

Our attempt to estimate the energetic profile of rotation of a vinyl-terminated polymer chain around the imaginary olefin-Zr axis utilized a coordinate drive calculation of the dihedral angle $\text{H-Zr-C}(1)_{\text{olefin}}\text{-C}(2)_{\text{olefin}}$ (cf. Figure 14). As set out above, the activation enthalpy for such a rotation was found to be about 2 kcal/mol. A local energy minimum is found for an ethene coordination mode perpendicular to the plane spanned by $\text{H-Zr-C}_{\text{olefin}}$ in the initial/end geometries and is possibly more stable than an in-plane coordination mode. Compared to the isomerization of agostic structures, this energy barrier is surprisingly low, indicating a strong likelihood of this process. The rotation allows a further energetic stabilization of the active site as species formed from such a rotation may form stable hydride-olefin complexes.

Consideration of the termination mechanism toward vinylidene moieties features a lower activation enthalpy of 14 kcal/mol to afford reaction products stabilized by 6 kcal/mol, which is clearly significant.

β -Hydride Transfer. The formation of vinyl and vinylidene chain terminations is usually assigned to BHT reactions. *Trans*-vinylene terminations can, however, not originate from hydride transfer reactions in the classical polymerization mechanisms.

TABLE 5: Transition State Energies for the Two Possible Terminations Arising from BHT in Ethene-*co*-1-hexene Polymerization and the Stabilities of the Products Relative to Their TS^a

Termination	Transition State (kcal·mol ⁻¹)	Product Stabilisation (kcal·mol ⁻¹)	Product (kcal·mol ⁻¹)
	11	-11	-4
	20	-20	-12

^a The starting complexes before BHT served as energetic reference points that were arbitrarily set to zero kcal/mol.

To compare the activation enthalpies of BHE and BHT processes for **1**, we have investigated these by DFT.

In contrast to studies conducted on unsubstituted Cp-based zirconocenes, BHT processes fail to prove favorable also for **1/MAO** (cf. Table 5). Note that the energy gap for BHT and BHE has narrowed significantly. Only the normally predominant vinyl termination can claim a significantly lower activation enthalpy than the corresponding BHE reaction. Polymerization studies conducted with **1/MAO** and **2/MAO** have shown respectable amounts of *trans*-vinylene and vinylidene terminations. The transition from predominantly vinyl terminations for **1/MAO** to predominantly *trans*-vinylene terminations for **2/MAO** is a strong indication that the change in steric demand is enhancing the energetic trends calculated for **1**.

Fly, Little Proton, Fly. Another route of isomerization in metallocene catalysis with considerable steric congestion has recently appeared in literature.²³ The discovery of the 1,4- σ -bond metathesis reaction for the C(7)-chain branching of norbornene invokes the question whether or not this route would be a viable reaction from the stable δ -agostic interaction **A(III)** that we have characterized computationally.

Construction of the possible transition state and relaxation of the ligand framework prior to the transition state search provided the transition states depicted in Figure 15. The activation enthalpy of 26.4 kcal/mol for the 1,4- σ -bond metathesis **STS 1** falls into the lower energy range for BHE processes. While such a process is unlikely to have any importance at low temperatures, it may gain significance as the temperature increases. Prior to the metathesis reaction, the C(1)–C(4) distance of the six-membered ring in chair conformation shortens from 3.2 to 3.0 Å, as the backbone assumes a synclinal conformation, which deviates by 23° from the perfectly staggered backbone arrangement.

The corresponding transition state for the 1,3- σ -bond metathesis reaction (**STS 2**) demands the contraction of the five-membered γ -agostic structure **A(II)** to the strongly strained four-membered zirconacycle (**STS 2**). The activation enthalpy for this geometry with a cis configuration of the geminal substituents calculates to 49.5 kcal/mol. This may be considered the lower limit, as the *trans* configuration causes more steric strain and favors to tilt out of the transition state plane. AMBER force field calculations of the constructed³⁰ and not optimized transition states predict a marginal stabilization of the cis configuration by less than 1 kcal/mol.

Consequently, we have attempted to design a 1,2- σ -bond metathesis reaction. The metathesis reaction product would show a geometry resembling that of **B(IV)**, which would readily undergo BHE to yield the observed *trans*-vinylene. For the 1,2- σ -bond metathesis, two geometrical arrangements of the transition state should be accessible, that is, front- and back-side transfer for the hydrogen (**STS 5** and **STS 4**, respectively, in

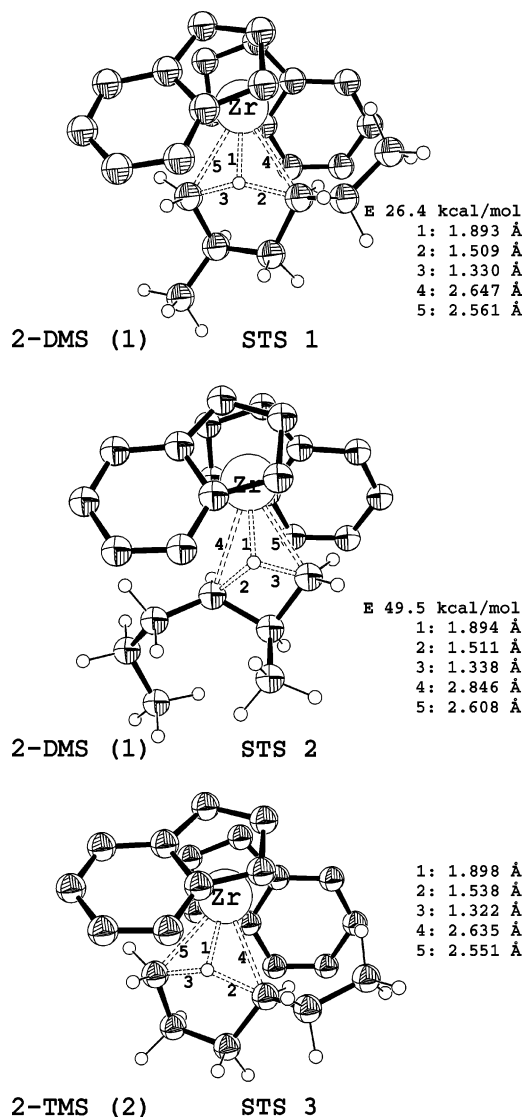


Figure 15. Transition state geometries for the 1,4- (STS 1, STS 3) and 1,3- σ -bond (STS 2) metathesis reactions of **1** and **2**. The silyl moieties and hydrogens on the catalyst are omitted for clarity. STS 1 and STS 3 are geometrically very similar. The transition state may be described as an envelope conformation of a five-membered ring. The C(1)–C(4) distance is shortened to 2.27 Å; the proton lies above the Zr–C(1)–C(4) plane at a distance of 1.89 Å to the zirconium atom, asymmetrically coordinated between the C(1) and C(4) at a distance of 1.33 and 1.51 Å, respectively. The branching product is less stable than the δ -agostic polymer chain by 4.9 kcal/mol.

Figure 16). While a Zr–H interaction would exist in the former case, a sterically less demanding configuration could be achieved by back-side transfer. From the point of view of electronic structure, the back-side metathesis is analogous to a 1,2-H-shift reaction in carbenium ions. The calculated energy of the front-side transition state is 65 kcal/mol. This high energy arises from a tilt movement of the polymer chain, so that both carbon atoms can interact intimately with the zirconium atom. The reaction product and its precursors are of similar stability. The back-side transition state is estimated to 34 kcal/mol, which is very close to the energy obtained for the 1,4- σ -bond metathesis route. It may be speculated that the energy calculated for STS 4 would in reality be further diminished by the type and nature of the solvent employed. A suitably electron-donating solvent (Lewis base) should in principle be able to stabilize transition state STS 4 better than an electron accepting solvent (Lewis acid).

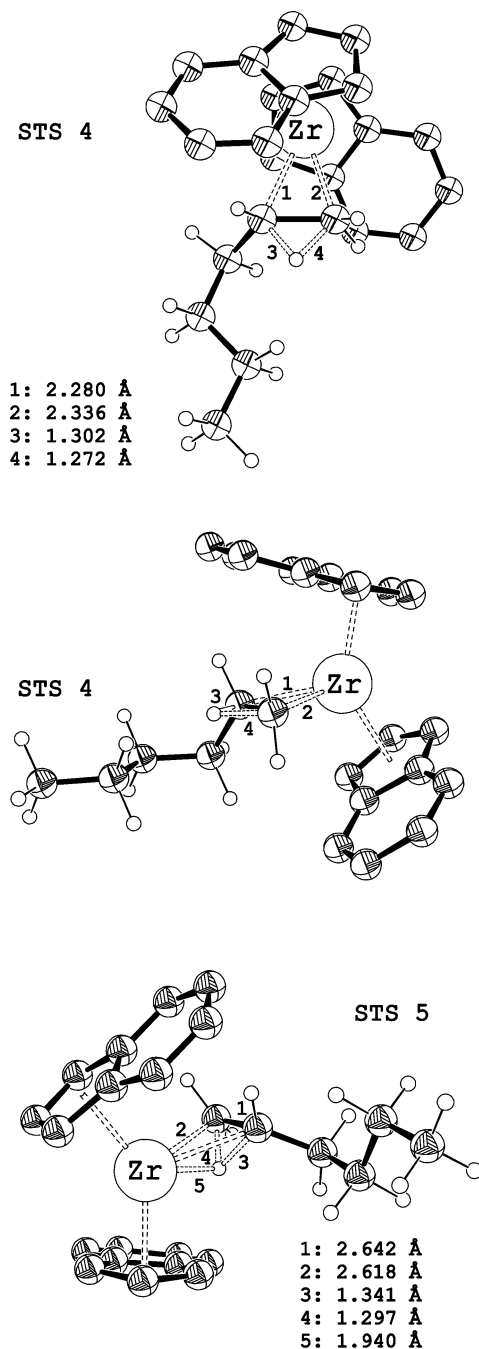


Figure 16. Transition state geometries for the 1,2-back-side (STS4) and 1,2-front-side (STS5) σ -bond metathesis reaction of **1**. The silyl moiety and some hydrogen atoms are omitted for clarity.

Both isomerization routes, 1,2- and 1,4- σ -bond metathesis, appear viable for 1/MAO. At the same time, the isomerization rate of 2/MAO is higher than that of 1/MAO. The investigation and comparison of a similar transition state of possibly lower energy for 2/MAO is therefore mandatory. Although the steric load of this system is higher, comparable energies are obtained with 30 kcal/mol for the transition state and 9.7 kcal/mol stabilization of the unbranched polymer chain. These energies suggest that 1,4- σ -bond metathesis has to be accounted for at elevated temperatures also for 2/MAO.

The transition state geometry for **2** is depicted in Figure 15 (STS 3) and is essentially identical with STS 1. A major difference can be seen in the start and end conformer of the reaction. As the dihedral angle φ of **1** changes from -100 to

−102° (STS 1) and further to −94°, the same angle changes in 2 from −105 to −102° (STS 3) and further to −86°. An outline of the metathesis reactions is given in Scheme 2.

Undesired Romances. During our studies of the numerous reactions of the active site we serendipitously discovered an unforeseen agostic interaction in coordinatively unsaturated or sterically less loaded active sites. Olefin and hydrido olefin complexes with a lateral oriented silyl substituent can tilt the silyl group into the interligand space and hence donate electron density back to the metal center. This ligand agostic interaction is characterized by a Si–H and Zr–H distance of 1.55 and 2.51 Å, respectively, which is an elongation of the Si–H bond by 0.05 Å. Several calculations with different starting geometries and at a higher level of theory, B3LYP/6-31G* instead of BP86/6-31G*, did not lead to any other result.

Ligand activation reactions have been experimentally observed, but those reports were on C–H activations in trimethylsilyl groups rather than Si–H activations.^{29–34} Because oxidative addition of C–H bonds to zirconium is known, a compelling question arises: Can a ligand be activated toward a Si–H bond cleavage and what would be the features of such a reaction?

Two coordinate drive calculations were conducted. The first started with the polymer chain β -agostic interaction oriented toward the agostic silyl group. The distance between the two agostic hydrogens was reduced in 0.2 Å steps, and full relaxation of the remaining structure was allowed for each step. The potential energy of these species increased sharply at a distance of 1.7 Å (Figure 17). The calculation was abandoned at a proton–proton distance of 1.12 Å, as rearrangement would apparently not occur.

Rotation of the polymer chain brought the zirconium carbon σ -bond into the proximity of the agostic silyl moiety. Prior to the second coordinate drive, a full relaxation of the geometry was allowed; an increase in the agostic interaction is notable and results in an energy gain of 1.1 kcal/mol. The Si–H bond lengthens by another 0.03 to 1.58 Å, whereas the Zr–H bond shortens significantly to 2.15 Å. The C–H_{Si} distance measures 2.71 Å. The potential energy plot presented in Figure 17 was obtained from a decrease of the C–H_{Si} bond by 0.2 Å steps. The transition state was estimated to display a hydrogen–carbon distance of 1.6 Å at an energy of approximately 16 kcal/mol. Our computed values for the H–X distances in the TS structure are 1.94 (Zr), 1.93 (Si), and 1.55 (C) Å with an energy of 14.0 kcal/mol. While the decrease of energy for the protonation of the anionic silicon is moderate, a steep decrease in energy is found for the protonation of the carbanion. Full relaxation of the alkane zirconium complex revealed a pronounced α,β -agostic interaction of the alkane, and carbon–zirconium distances typical for olefin complexes (DC1, Figure 18). The alkane C–H bonds are stretched to 1.13 Å and the C(1)–Zr and C(2)–Zr distances measure 2.78 and 2.90 Å, respectively. The structural changes of the zirconium complexes are characterized by a shortening of the C(2)–Si bond from 1.91 to 1.87 Å and is accompanied by inversion of the out-of-plane bend direction of the silyl moiety with respect to the Cp ring. The angle Si–C(2)–Cp_{centroid} for the unaffected silyl moiety measures 16.7° and is oriented away from the interligand space. In contrast, the deprotonated silyl group is bent toward the zirconium into the interligand space by 34.6°. The Zr–Si distance is as short as 2.80 Å, indicating electron donation from silicon to zirconium. The deprotonated ligand has moved toward the silicon along the Si–C(2) axis and coordination by the Cp-moiety is less symmetrical. This arrangement is destabilised with 3.2 kcal/mol relative to the agostic interaction of the protonated ligand.

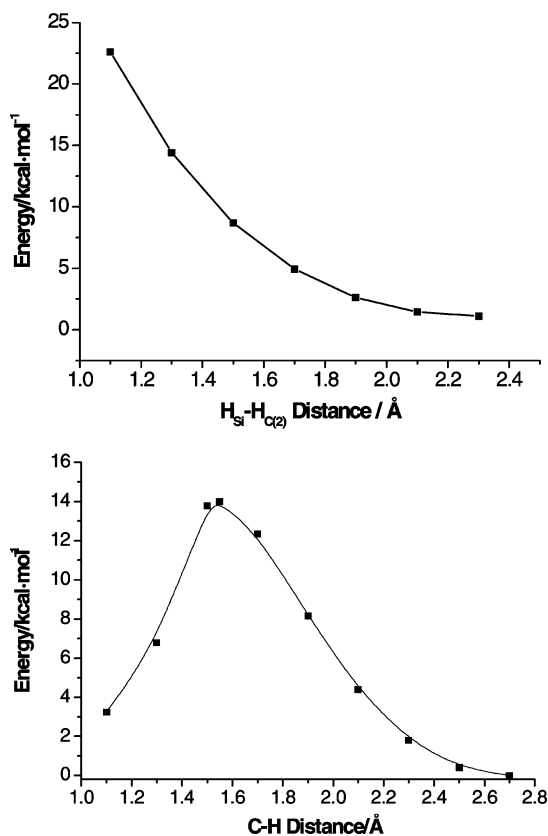


Figure 17. The upper graph shows the potential energy profile for the approach of the silyl-proton to the β -agostic proton of the polymer chain to investigate possible though unlikely elimination of hydrogen. The movement is moderately restricted down to a distance of 1.7 Å. The lower potential energy profile describes the intramolecular deprotonation of the silyl-substituted ligand as a function of the C–H distance. The transition state was located at a C–H distance of 1.55 Å and estimated to 14.0 kcal/mol. All energies are referenced to the lowest energy computed that was arbitrarily set to zero kcal/mol.

The agostic interaction of the alkane is likely to stabilize the cationic zirconium center electronically, but upon removal of the alkane a steric stabilization by 13 kcal/mol became evident as well (DC2, Figure 18).³⁵ The separation of steric from electronic stabilization was achieved by separation of the alkane ligand from the catalyst and subsequent calculation of the difference of single point energies and energies after free relaxation. Free relaxation of the deprotonated zirconocene induced significant changes in the intact ligand: While the deprotonated ligand does not undergo further structural changes, the intact ligand bends around the C(3a)–C(7a) axis by 33.6° and moves along the Si–C(2) axis into the opposite direction. Hence, the benzo moiety of the indenyl ligand can contribute its electrons to stabilize the cationic center. The centroids for the Cp and benzo moieties are as close as 2.23 and 2.12 Å, the Zr–C distances get as short as 2.34 Å for the protonated and 2.41 Å for the deprotonated ligand. A relief in steric congestion causes the protonated silyl group to assume a nearly perfect in-plane position. Accounting for the fact that all potential electron donors are at maximum 2.8 Å away from the zirconium center and regarding the benzo moiety as being coordinated in a η^4 -mode, this complex could formally be considered an 18 valence electron species. Analysis of the change in Mulliken atomic charges during the reaction of this species suggests a clear increase in electron density on the zirconium atom and an equally clear decrease on silicon. The benzo moiety is, however, not unambiguously coordinated in a η^4 -mode.

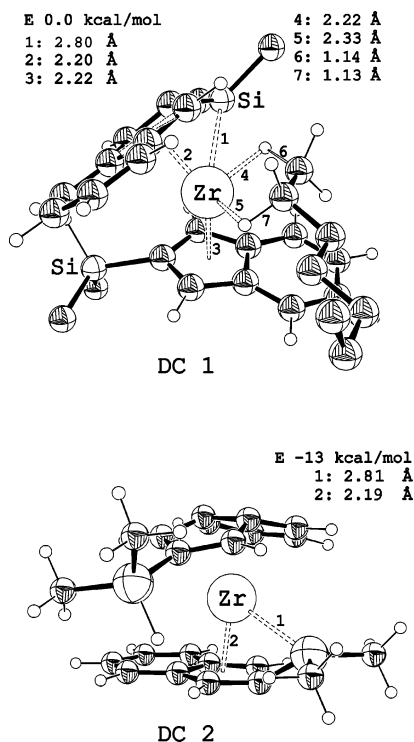


Figure 18. Simplified illustration of the α,β -agostic interaction of the alkane complex **DC1** and the fully relaxed, deprotonated complex **DC2** after removal of the alkane ligand. Some hydrogen atoms are omitted for clarity.

To consider the effect of the solvent on the complex after dissociation of the alkane, an optimization was started from a structure in which a toluene molecule was placed in a distance of 4 Å away from the zirconium atom. Full optimization of the assembly resulted in association of the toluene in an unsymmetric and rather ill-defined manner. The π -electron system was not completely oriented toward the zirconium center, but approached it slightly tilted. We could not find indications for C–H activation as the bond lengths remain essentially unchanged. Comparison of the energy of free toluene with the energy of the unrelaxed and relaxed complexes suggests that toluene acts mainly as a steric stabilizer. Both complexes, the toluene coordinating and the fully optimized **DC2**, are distinguished by a energy difference of 0.6 kcal/mol, which is within the computational error margin.

The reaction profile for association of ethene to **DC3** is shown in Figure 19. Proceeding in the same fashion as before, the olefin was placed 4 Å away from the zirconium center as depicted in Figure 20. Full optimization afforded the symmetrically coordinated π -complex **DC4** after few cycles. The potential energy profile shown in Figure 19 reveals no local minimum but a shoulder in the energy curve for this complex in the free relaxation. At this stage of the reaction, the complex has gained approximately 13 kcal/mol (**DC4**), which likely accounts for its steric and electronic stabilization. Because of the small gradient on this shoulder, the reaction readily continued with slow displacement of the ethene unit toward the silicon anion. The insertion provides the liberation of another 18 kcal/mol. Because of the absence of an activation barrier at this level of theory, ethene enchainment is a strictly exothermic process with a change in energy of 30 kcal/mol.

Olefin Enchainment. The discrimination of the several relevant conformers among the less likely ones is a major

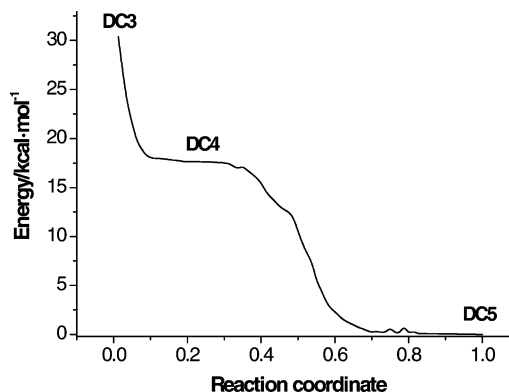


Figure 19. The potential energy profile for the reaction of **DC2** with ethene does not show a local minimum for the π -complex, but proceeds through the shoulder (**DC4**) with insertion of the ethene molecule into the Zr–Si bond (**DC5**). The reaction coordinate is defined by the sequence of geometries in the course of the calculation. The lowest energy computed was arbitrarily set to zero kcal/mol.

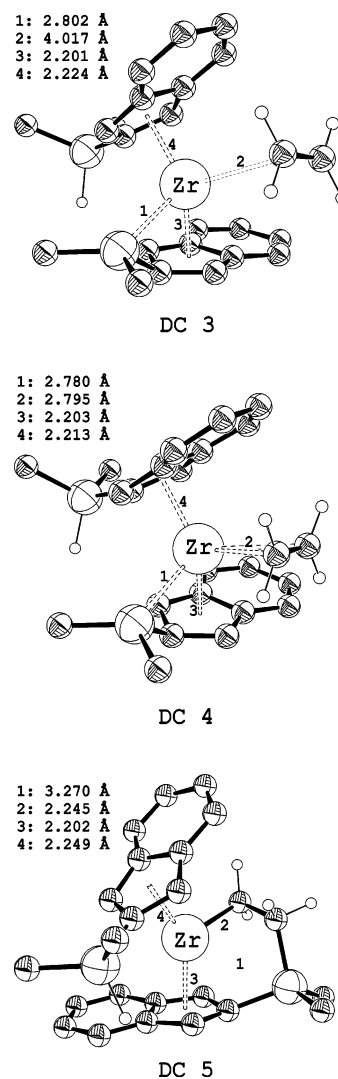


Figure 20. The three key structures **DC3**, **DC4**, and **DC5** of the free relaxation calculation of **DC1** after substitution of the alkane by a remote ethene molecule. Note the upper, deprotonated indenyl ligand's Cp moiety swings toward the zirconium center; the lower ligand does not move for the transition **DC3** to **DC4**.

prerequisite if the theoretical description of olefin enchainment in dual-side zirconocenes is to be successful. We have calculated a possible transition state geometry of the insertion and used the frozen transition state core in a force field scan of the two-

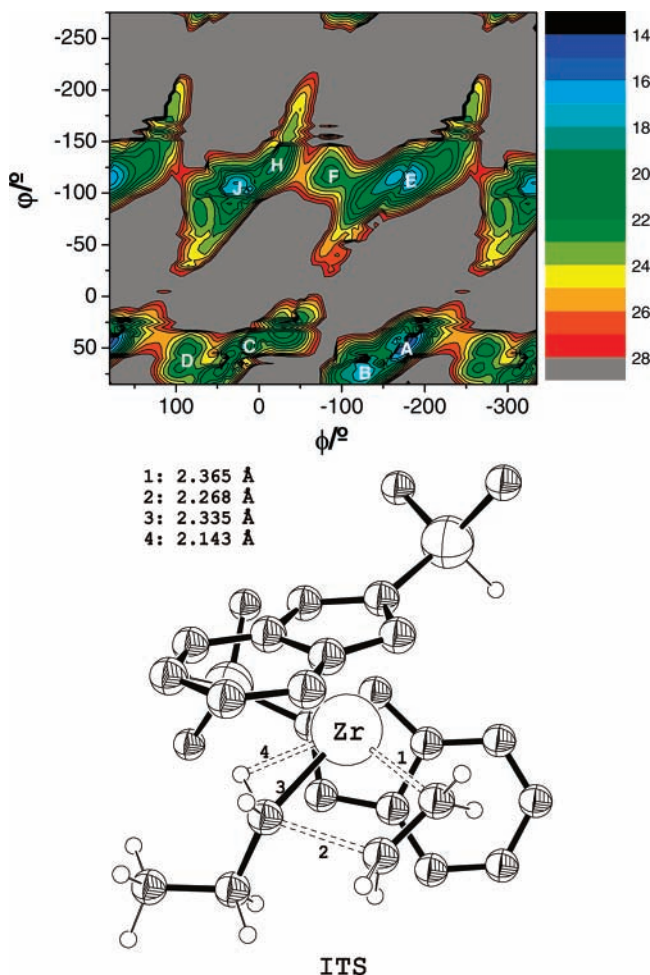
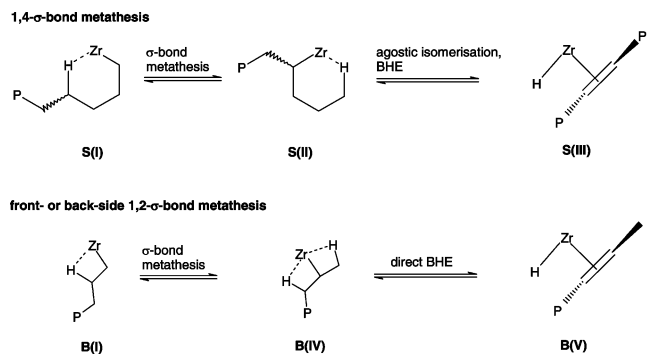


Figure 21. Potential energy surface for the transition state of olefin insertion; front-side attack with α -agostic interaction of the polymer chain. The energy cutoff is set to 28 kcal/mol. The local minimum **A** and the global minimum **H** belong to the meso- and rac-like series of transition states. **ITS** represents a typical “frozen transition state” geometry as applied during this MM-study.

dimensional potential energy surface, as we did before for the dichlorides. The energies obtained from this type of calculation should be interpreted with some reservation, but the energy minima should give a good hint to the relevant geometries. The result of the computations for ethene insertion into a linear polymer chain with a α -agostic interaction is visualized in **ITS** in Figure 21. The four geometries **A–D** belong to synclinal meso-like conformers, whereas **E–J** are synclinal with both silyl substituents pointing backward (Figure 21). Among these two types of conformation, the variation of the individual geometry parameters is minimal. The two minima **A** and **E** show identical energies in the AMBER force field, and the global minimum is found for **H** after manual reorientation of the DMS group.

Transition state searches for all eight conformers for this simple case of olefin enchainment were initiated. We experienced severe convergence difficulties in the geometry optimizations, undoubtedly because of the very small energies required to accomplish large deformations of parts of the molecular system. The calculations were rather prone to displacement effects in the sloppy polymer chain which effectively precluded investigation of the different insertion steps at reasonable computational costs. A further consideration of other possible transition state geometries for insertion, featuring for instance discrimination of front- and back-side attack, were therefore omitted.

SCHEME 2: General Mechanistic Outline of Internal Double Bond Formation by σ -bond Metathesis Reactions^a



^a The 1,4- σ -bond metathesis (**S(I)**–**S(III)**) starts from an energetically favorable δ -agostic interaction (**A(III)**). 1,2- σ -bond metathesis starts from the β -agostic interaction **A(I)** and would favor a back-side isomerization. Note that the final BHE would occur spontaneously, *vide infra*.

Conclusions

The experimental data obtained from homopolymerizations with bis(2-DMS-ind)zirconium(IV) dichloride (**1**)/MAO and bis(2-TMS-ind)zirconium(IV) dichloride (**2**)/MAO reveals a decay in activity with increasing temperature for both systems. The end group analysis as a function of the temperature suggests the presence of chain transfer to aluminum, which seem to be favored at lower temperatures because of the bimolecular nature of this reaction. The pronounced temperature dependence of the ratio of *trans*-vinylene to vinyl terminations is found to increase with steric congestion at the active site. The molecular weights of the polymers obtained at moderate temperatures are high, indicating little significance of BHT. These findings are in agreement with theoretical predictions of the relative changes in propagation and termination rates for bimolecular processes, compared to the uni-molecular termination by BHE.²⁷ This is further supported by present computational results. The polydispersity indices of the polymers increase with temperature and multisite behavior has to be assumed. The assessment of the conformational space of **1** and **2** displays a rather low isomerization barrier of approximately 6 kcal/mol. Because polymer chains generally require less space at the active site than the chloride ligands of the catalyst precursor, it may be speculated that a larger number of sites becomes thermodynamically accessible with increasing temperature.

The copolymerizations of ethene and 1-hexene were conducted with **1**/MAO and investigated as a function of the comonomer mole fraction in the feed. Two series were run of which the series at a temperature of 30 °C is difficult to evaluate because of dissatisfactory reproducibility. Depleting Soxhlet extraction of an apparently bimodal polymer blend afforded six fractions of which five could be more thoroughly examined. Interestingly, two fractions displayed different solubilities but identical molecular weights. The high comonomer content of the lowest molecular weight fraction compared to the highest molecular weight fraction, as determined by ¹³C NMR analysis, clearly illustrates the multisite character of **1**/MAO. Fitting of experimental melting points (DSC) with theoretical ones for a homogeneous comonomer and polymer distribution was conducted. The poor agreement between theoretical and experimental data further supports the claim that the copolymer is not of homogeneous composition and that the distribution of the comonomer along the chain does not necessarily result from a stationary polymerization process. We believe that this last characteristic arises from the very short polymer chains, which

allow no statistical distribution at the extremely low comonomer incorporations observed.

The theoretical investigation of **1** and **2** has been attempted at two different levels. Mapping of the potential energy surface of the dichlorides with respect to two degrees of freedom has been achieved by means of force field calculations. These show transition states for the synperiplanar (meso-like) conformer, though the minima of the synclinal, synperiplanar, and anti-periplanar (rac-like) are energetically degenerate. The activation enthalpy for a rac/meso interconversion of **2** is somewhat higher than for **1**, and a limited accessibility of the different conformers must be assumed for **2**. Verification of the exact locations of minima and maxima on the potential energy surface has been attempted using B3LYP/6-311G** single point energy calculations. A significant failure of the AMBER force field was found in the location of periplanar conformers. The relative activation enthalpies were in reasonably good agreement, that is, ± 2 kcal/mol. Excellent agreement has been found for single point energies obtained from calculations at the B3LYP/6-31G*, B3LYP/6-311G**, and MP2/6-31G* levels of theory.

More sophisticated investigations on 1/MAO were started to account for the different reaction and isomerization pathways of the active site in the course of homo- and copolymerizations. Investigation of agostic structure interconversions in this sterically demanding system found the δ -agostic polymer chain interaction to be lowest in energy, which is in contrast to the results obtained by Ziegler et al. for less sterically strained bis-Cp-based systems. For 1/MAO, the β -agostic interaction is most likely the least populated species accounting for the relative energies of stationary points and transition states under both conditions, high and low propagation rate. The relative energies of the agostic isomers reported here indicate that the β -agostic species will not be strongly populated, even under polymerization conditions that allow for equilibration of the agostic interactions. The high degree of end group isomerization for 1/MAO and 2/MAO demands viability of BHE if the classical mechanism is to be valid. In contrast to literature studies conducted on unsubstituted Cp-systems, we find that BHE and BHT processes display very similar activation enthalpies between 11 and 20 kcal/mol. The mechanisms of formation of vinylidene terminations could not be distinguished energetically in the DFT calculations. This finding is supported by experimental polymerization results, which clearly favor BHE termination products over BHT products for **2**. This is in agreement with our earlier studies on the carbon analogue of **2**, bis(2-*tert*-butylindenyl)zirconium(IV) dichloride, that does not feature chain termination by BHT at all due to steric congestion.²⁸

We have investigated an alternative mechanism, which does not require BHE reactions and proceeds as an unimolecular σ -bond metathesis. Of the 1,2-, 1,3-, and 1,4- σ -bond metatheses reactions under consideration, the back-side 1,2- and the front-side 1,4- σ -bond-metathesis fall into a thermodynamically accessible energy range from 34 to 30 kcal/mol, respectively. Because of the lower activation enthalpies estimated for BHE and BHT mechanisms, these reactions can be ruled out as the predominant mechanism. Nevertheless, these processes may also account for chain branching effects in other catalyst systems, where methyl and propyl branches occur, but the activation enthalpy for these reactions would have to be estimated individually.

The presently reported silyl group activation with a transition state energy of 14 kcal/mol in the course of polymerization is a rather undesirable feature of 1/MAO but may help to explain the short lifetime of the active species in the presence of ethene,

as indicated by rapid activity decay. The strongly distorted geometry **DC2** is not necessarily of physical relevance as solvent molecules appear to have a stabilizing effect. Dissociation of a stabilizing ligand will result in strong deformation of the ligand framework, which is left inert toward ethene. The exothermal character of this deformation may very well be reversible under polymerization conditions, but calculations hint at an exceedingly high reactivity of the resulting, unstabilized species. Ethene is readily inserted into the zirconium–silicon bond, which indicates the possibility of enchainment of the ligand framework. The question of whether this species is prone to decomposition or will enable further polymerization has not been investigated.

Because the agostic interactions of the polymer chain do not follow the behavior that may be anticipated from earlier works, we have embarked on the discrimination of active site conformers. More profound information on this detail of the active site may support the model of a multisite metallocene, as the circumstantial evidence from the polymerization experiments suggests. Unfortunately our attempts to quantify the activation enthalpies by means of DFT have been in vain because of computational difficulties.

The calculated activation energy for conformational change of the dichloride form of the catalyst is 6 kcal/mol. The activation energy for olefin insertion starting from the olefin complex is calculated to 2 kcal/mol. If we crudely estimate frequency factors of 3×10^{11} and 5×10^{12} , respectively, for the two processes, a simple Arrhenius expression gives rate constants of roughly 5×10^7 and 3×10^{11} for rotation and insertion, respectively, a difference in rate constants of 4 orders of magnitude. We conclude that insertion is much faster than rotation, which is entirely in line with a multisite catalyst hypothesis and the observed polydispersities of the polymer.

Accounting for all the experimental and theoretical data presented herein, we suggest that zirconocene catalysts of the type 1/MAO and 2/MAO are multisite zirconocenes. In contrast to Waymouth, we do not believe that low molecular weight fractions and large polydispersity indices arise from polymerization active decomposition products.¹² Though the systems under investigation differ distinctly from Waymouth's system,^{3a} the macroscopic behavior of the copolymerisates seems fairly alike. The reproducibility, the temperature dependence of the end groups, and energy profiles presented allow us to rationalize the experimental observations without assuming the existence of polymerization active decomposition products. The difficulties that we encountered in the interpretation of the GPC analyses of the copolymerization products formed at 30 °C were apparently not an issue in the case of Waymouth's systems. We believe that these difficulties arise because of the tremendous inhomogeneity of the polymer blends rather than experimental design. This may serve as a case for the use of different analysis methods when investigating these multisite catalysts that afford polymer products of large polydispersities.

Experimental Section

General Comments. The zirconocene dichlorides employed in this study were prepared as published elsewhere.^{10a} Toluene (Aldrich Chemicals) was dried over sodium /anthracene and distilled under nitrogen before use. Methylaluminoxane (MAO) as a 10% solution in toluene (Albemarle) was used as received. Ethene and 1-hexene of polymerization grade was received from Borealis Stathelle, Norway. High-temperature ¹³C NMR spectra were acquired on a Varian Gemini or VXR300 instrument operating at 75 MHz and were referenced to the residual solvent peaks. Typical acquisition parameters for quantitative analysis:

d1 = 10 s, 5000 scans, $T = 130$ °C, WALZ16 decoupling sequence, 50 mg polymer in 700 mg [D₄]ODCB, 5 mm probe. Weight and number average molecular weight distributions of the polymers blends were measured at 145 °C on a Polymer Labs PL-GPC210 instrument equipped with two PLgel 20 μ m MIXED-A LS 300 \times 7.5 mm columns and a 20 μ m precolumn. A Viscotek 210 RI dRI detector, a Vicotek 210RI four-capillary bridge viscometer, and a PD2040 light-scattering detector were employed. 1,2,4-Trichlorobenzene was used as solvent at a rate of 1.0 cm³ min⁻¹. The instrument was universally calibrated with narrow molecular weight polystyrene standards (Polymer Laboratories) in the range 1×10^3 to 2×10^7 g/mol. Weight and number average molecular weights and molecular weight distributions of the fractionated blend were measured at 140 °C with a Waters Alliance 2000 size exclusion chromatography (SEC) instrument equipped with Waters HT3, HT4, HT5, and HT6 columns. 1,2,4-Trichlorobenzene was used as solvent at a flow rate of 1.0 cm³ min⁻¹. The columns were universally calibrated with narrow molecular weight polystyrene standards. DSC analysis was conducted on a Perkin-Elmer DSC7 instrument calibrated with a N519-0762 calibration set. The scanning cycles used covered the temperature range from 40 to 180°. Cycle details: first heating rate 50 °C/min, 1 min equilibration, cooling rate 10 °C/min, 3 min equilibration, second heating rate 10 °C/min. Melting points and enthalpies were determined from the second cycle. FT-IR analyses were conducted in vacuo on a Bruker IFS 66v instrument, typically with 200 scans.

Polymerization Procedure. A 250 mL steel autoclave was heated to 350 °C for 60 s prior to evacuation/flushing period of 30 min with four cycles of flushing with nitrogen. The reaction vessel was then heated to the experiment temperature, filled with toluene (200 mL), and the appropriate volume of comonomer if necessary. MAO solution was injected through a septum via syringe and pressurized with ethene until gas- and liquid-phase had equilibrated. The polymerization reaction was initiated by addition of a dilute solution of the zirconocene dichloride in toluene. At the end of the reaction, the active species was quenched by addition of methanol (20 mL), then the reaction slurry was transferred into a mixture of methanol and hydrochloric acid (10:1, 300 mL). Stirring overnight, filtration and washing with methanol was followed by drying under ambient conditions, and selected samples were dried in vacuo.

Computational Details. DFT calculations were performed with the Gaussian 03 package.³⁷ The BP86 functional with the 6-31G* basis set was employed and proved to be suitable.³⁸ For Zr, a modified version of the LANL2DZ ECP basis was used.³⁹ In the original Zr basis set, the 4d shell is described by two contracted Gaussians of which one is contracted from three primitive functions and the other is a single primitive function. To increase flexibility in the d shell, we decontracted the set to three functions, consisting of two, one, and one primitive functions, respectively. Default settings were used for all parameters except for the integration grid, which was set to "ultrafine". Geometry optimizations and transition state searches were conducted using the density fitting approximation with auxiliary basis sets as implemented.⁴⁰ Unexpected results obtained from these calculations have been verified by calculations without the density fitting approximation and eventually with calculations employing the B3LYP hybrid functional. All transition states have been subjected to analytical frequency calculations and showed only one imaginary frequency in the vibrational spectrum. To verify that computed transition states connected the desired local energy minima, the TS geometry

was perturbed slightly toward the minima and geometry relaxations performed. All transition state searches started from geometries constructed by means of force field calculations.

AMBER force field calculations were performed with Hyperchem 7.1, student edition. A modification of the force field used by Brintzinger et al.¹⁹ proved necessary for our purpose, but the data obtained from these calculations requires careful scrutiny. The two-dimensional potential energy surfaces of the dichlorides contain the contribution of the restraints to the total energy after complete relaxation of the molecule. For the active site, a DFT-optimized transition state geometry was used. The different conformers were calculated with frozen coordinates of the transition state core. As the optimization was carried out with this restraint, the energy surface is biased by the energetic contribution of the frozen transition state.

All illustrations of molecular geometries obtained from calculations were made using MOLEKEL.⁴¹

Acknowledgment. We would like to thank Aud M. Bouzga for assistance with the multinuclear NMR experiments and Dr. Knut Thorshaug for fruitful discussions. Dr. Frank Schaper's help with the initial setup of the AMBER force field in Hyperchem is very much appreciated. This research was generously supported by the Research Council of Norway through a Dr.-Ing. scholarship (to A.C.M., Grant 145544/431) and the European Science Foundation through a COST Action D17 short-term scientific mission (STSM) grant (to A.C.M., reference codes COST-STSM-D17-00069 and COST-STSM-D17-00070). A.C.M gratefully appreciates the critical discussions with Professor Dr. Walter Thiel, PD Dr. Klaus Angermund, Dr. Martin Graf, Dr. Stephan Thiel, and Dr. Holger Hermann and their hospitality during the STSM stays. Generous grants of computing time at the HPC facilities at the University of Oslo by NOTUR (Grant nn2969k) and at the Norwegian University of Science and Technology (NTNU) Trondheim by the BFU-council (Grant ntnu106) were crucial for the conduction of this work. We are indebted to Dr. Richard H. Heyn for his careful proofreading of the manuscript.

Supporting Information Available: Cartesian geometry files of all relevant structures, including transition states, DFT and MM calculations, and the AMBER force field parameter file are deposited in electronic form. A comparison of the 1-hexene incorporations as determined by FT-IR and ¹³C NMR is listed. This material is available free of charge via the Internet at <http://pubs.acs.org>.

References and Notes

- (1) (a) Sinn, H.; Kaminsky, W. *Adv. Organomet. Chem.* **1980**, *18*, 99–149. (b) Wild, F. R. W. P.; Zsolnai, L.; Huttner, G.; Brintzinger, H. H. *J. Organomet. Chem.* **1982**, *232*, 233–247. (c) Ewen, J. A. *J. Am. Chem. Soc.* **1984**, *106*, 6355–6364. (d) Kaminsky, W.; Külper, K.; Brintzinger, H. H.; Wild, F. R. W. P. *Angew. Chem., Int. Ed. Engl.* **1985**, *24*, 507–508.
- (2) (a) Bochmann, M. *J. Chem. Soc., Dalton Trans.* **1996**, 255–270. (b) Coates, G. W. *Chem. Rev.* **2000**, *100*, 1223–1252.
- (3) (a) Coates, G. W.; Waymouth, R. M. *Science* **1995**, *267*, 217–219. (b) Bruce, M. D.; Coates, G. W.; Hauptman, E.; Waymouth, R. M.; Ziller, J. W. *J. Am. Chem. Soc.* **1997**, *119*, 11174–11182. (c) Kravchenko, R.; Masood, A.; Waymouth, R. M. *Organometallics* **1997**, *16*, 3635–3639. (d) Kravchenko, R.; Masood, A.; Waymouth, R. M.; Myers, C. L. *J. Am. Chem. Soc.* **1998**, *120*, 2039–2046. (e) Witte, P.; Lal, T. K.; Waymouth, R. M. *Organometallics* **1999**, *18*, 4147–4155. (f) Wilmes, G. M.; France, M. B.; Lynch, S. R.; Waymouth, R. M. *Organometallics* **2004**, *23*, 2405–241.
- (4) (a) Busico, V.; Cipullo, R.; Segre, A. L.; Talarico, G.; Vacatello, M.; Van Axel Castelli, V. *Macromolecules* **2001**, *34*, 8412–8415. (b) Busico, V.; Cipullo, R.; Kretschmer, W.; Talarico, G.; Vacatello, M.; Van Axel Castelli, V. *Angew. Chem., Int. Ed.* **2002**, *41*, 505–508.

- (5) Foster, P.; Chien, J. C. W.; Rausch, M. D. *Organometallics* **1996**, *15*, 4951–4953.
- (6) Leino, R. P.; Luttikhedde, H.; Wilén, C.-E.; Sillanpää, R.; Näsman, J. H. *Organometallics* **1996**, *15*, 2450–2453.
- (7) (a) Knüppel, S.; Fauré, J.-L.; Erker, G.; Kehr, G.; Nissinen, M.; Fröhlich, R. *Organometallics* **2000**, *19*, 1262–1268. (b) Luttikhedde, H. J. G.; Leino, R. P.; Ahlgrén, M. J.; Pakkanen, T. A.; Näsman, J. H. *J. Organomet. Chem.* **1998**, *557*, 227–230. (c) Luttikhedde, H. J. G.; Leino, R. P.; Wilén, C.-E.; Näsman, J. H.; Ahlgrén, M. J.; Pakkanen, T. A. *Organometallics* **1996**, *15*, 3092–3094.
- (8) (a) Dreier, T.; Erker, G.; Fröhlich, R.; Wibbeling, B. *Organometallics* **2000**, *19*, 4095–4103. (b) Dreier, T.; Unger, G.; Erker, G.; Wibbeling, B.; Fröhlich, R. *J. Organomet. Chem.* **2001**, *622*, 143–148. (c) Dreier, T.; Bergander, K.; Wegelius, E.; Fröhlich, R.; Erker, G. *Organometallics* **2001**, *20*, 5067–5075.
- (9) (a) Grimmer, N. E.; Coville, N. J.; de Koning, C. B.; Smith, J. M.; Cook, L. M. *J. Organomet. Chem.* **2000**, *616*, 112–127. (b) Grimmer, N. E.; Coville, N. J.; de Koning, C. B. *J. Organomet. Chem.* **2002**, *642*, 195–202.
- (10) (a) Möller, A. C.; Heyn, R. H.; Blom, R.; Swang, O.; Görbitz, C. H.; Kopf, J. *Dalton Trans.* **2004**, 1578–1589. (b) Hannisdal, A.; Möller, A. C.; Rytter, E.; Blom, R. *Macromol. Symp.* **2004**, *213*, 79–88.
- (11) Wester, T. S.; Johnsen, H.; Kittilsen, P.; Rytter, E. *Macromol. Chem. Phys.* **1998**, *199*, 1989–2004.
- (12) Hung, J.; Cole, A. P.; Waymouth, R. M. *Macromolecules* **2003**, *36*, 2454–2463.
- (13) (a) Margl, P.; Deng, L.; Ziegler, T. *J. Am. Chem. Soc.* **1999**, *121*, 154–162. (b) Woo, T. K.; Fan, L.; Ziegler, T. *Organometallics* **1994**, *13*, 2252. (c) Talarico, G.; Blok, A. N. J.; Woo, T. K.; Cavallo, L. *Organometallics* **2002**, *21*, 4939–4949.
- (14) Quijada, R.; Dupont, J.; Miranda, M. S. L.; Scipioni, R. B.; Galland, G. B. *Macromol. Chem. Phys.* **1995**, *196*, 3991–4000.
- (15) (a) Reybuck, S. E.; Meyer, A.; Waymouth, R. M. *Macromolecules* **2002**, *35*, 637–643. (b) Hung, J.; Cole, A. P.; Waymouth, R. M. *Macromolecules* **2003**, *36*, 2454–2463.
- (16) (a) Resconi, L.; Jones, R. L.; Rheingold, A. L.; Yap, G. P. A. *Macromolecules* **1996**, *15*, 998–1005. (b) Stehling, U.; Diebold, J.; Kirsten, R.; Röhl, W. R.; Brintzinger, H. H.; Jüngling, S.; Müllhaupt, R.; Langhauser, F. *Organometallics* **1994**, *13*, 964–970. (c) Blom, R.; Follestad, A.; Noel, O. *J. Mol. Catal.* **1994**, *91*, 237–249. (d) Kissin, Y. V. In *Organometallic Catalysts and Olefin Polymerization*, Blom, R., Follestad, A., Rytter, E., Tilset, M., Ystenes, M., Eds.; Springer: Berlin, 2001; pp 213–228.
- (17) (a) Flory, P. J. *Principles of polymer chemistry. Phase equilibria in polymer systems*; Cornell University Press: Ithaca, NY, 1953; pp 541–594. (b) Tangen, L. Hovedoppgave, NTNU, Trondheim, Norway, 1999.
- (18) (a) Burger, B. J.; Thompson, M. E.; Cotter, W. D.; Bercaw, J. E. *J. Am. Chem. Soc.* **1990**, *112*, 1566–1577. (b) Alelyunas, Y. W.; Guo, Z.; LaPointe, R. E.; Jordan, R. F. *Organometallics* **1993**, *12*, 544–553. (c) Hajela, S.; Bercaw, J. E. *Organometallics* **1994**, *13*, 1147–1154. (d) Guo, Z.; Swenson, D. C.; Jordan, R. F. *Organometallics* **1994**, *13*, 1424–1432.
- (19) Schneider, N.; Schaper, F.; Schmidt, K.; Kirsten, R.; Geyer, A.; Brintzinger, H. H. *Organometallics* **2000**, *19*, 3597–3604.
- (20) Pietsch, M. A.; Rappé, A. K. *J. Am. Chem. Soc.* **1996**, *118*, 10908–10909.
- (21) Scherer, W.; McGrady, G. S. *Angew. Chem., Int. Ed.* **2004**, *43*, 1782–1806.
- (22) (a) Lohrenz, J. C. W.; Woo, T. K.; Ziegler, T. *J. Am. Chem. Soc.* **1995**, *117*, 12793–12800. (b) Margl, P.; Lohrenz, J. C. W.; Ziegler, T.; Blöchl, P. E. *J. Am. Chem. Soc.* **1996**, *118*, 4434–4441. (c) Margl, P.; Deng, L.; Ziegler, T. *Organometallics* **1998**, *17*, 933–946.
- (23) Karafilidis, C.; Hermann, H.; Ruffińska, A.; Gabor, B.; Mynott, R. J.; Breitenbruch, G.; Weidenthaler, C.; Rust, J.; Joppek, W.; Brookhart, M. S.; Thiel, W.; Fink, G. *Angew. Chem.* **2004**, *116*, 2498–2500.
- (24) (a) Govind, N.; Andzelm, J.; Reindel, K.; Fritzgerald, G. *Int. J. Mol. Sci.* **2002**, *3*, 423–434. (b) Thibault-Starzyk, F.; Vimont, A.; Fernandez, C.; Gilson, J. P. *Chem. Commun.* **2000**, 1003–1004. (c) Wang, D. J.; Lunsford, J. H.; Rosynek, M. P. *Top. Catal.* **1996**, *3*, 289–297. (d) Song, F.; Cannon, R. D.; Bochmann, M. *J. Am. Chem. Soc.* **2003**, *125*, 7641–7653. (e) Landis, C. R.; Sillars, D. R.; Batterton, J. M. *J. Am. Chem. Soc.* **2004**, *126*, 8890–8891.
- (25) (a) Thorshaug, K.; Rytter, E.; Ystenes, M. *Macromol. Rapid Commun.* **1997**, *18*, 715–722. (b) Thorshaug, K.; Støvneng, J. A.; Rytter, E.; Ystenes, M. *Macromolecules* **1998**, *31*, 7149–7165.
- (26) Støvneng, J. A.; Rytter, E. *J. Organomet. Chem.* **1996**, *519*, 277–280.
- (27) (a) Woo, T. K.; Fan, L.; Ziegler, T. *Organometallics* **1994**, *13*, 2252–2261. (b) Lohrenz, J. C. W.; Woo, T. K.; Fan, L.; Ziegler, T. *J. Organomet. Chem.* **1995**, *497*, 91–104.
- (28) Möller, A. C.; Blom, R.; Heyn, R. H.; Swang, O.; Kopf, J.; Seraidaris, T. *Dalton Trans.* **2006**, 2098–2105.
- (29) (a) Pool, J. A.; Lobkovsky, E.; Chirik, P. J. *Organometallics* **2003**, *22*, 2797–2805. (b) Bradley, C. A.; Lobkovsky, E.; Keresztes, I.; Chirik, P. J. *J. Am. Chem. Soc.* **2005**, *127*, 10291–10304. (c) Bradley, C. A.; Keresztes, I.; Lobkovsky, E.; Young, V. G.; Chirik, P. J. *J. Am. Chem. Soc.* **2004**, *126*, 16937–16950.
- (30) The construction of transition states in the force field was achieved by restraining crucial distances, for example, Zr–C(1), Zr–C(3), C(1)–C(3), Zr–H, C(1)–H, and C(3)–H, and where necessary angles and dihedrals to values for similar bonding situations as observed by means of XRD or DFT. Force constants for such constructions were set as high as possible and varied until the transition state met all demands of chemical intuition. The obtained geometry was then subjected to DFT transition state searches. These results may in turn be used for a “frozen transition state” in future force field design.
- (31) Choukroun, R.; Wolff, F.; Lorber, C.; Donnadiu, B. *Organometallics* **2003**, *22*, 2245–2248.
- (32) (a) Yang, X.; Stern, C. L.; Marks, T. J. *J. Am. Chem. Soc.* **1991**, *113*, 3623–3625. (b) Yang, X.; Stern, C. L.; Marks, T. J. *J. Am. Chem. Soc.* **1994**, *116*, 10015–10031.
- (33) Horton, A. D. *Organometallics* **1992**, *11*, 3271–3275.
- (34) Bochman, M.; Lancaster, S.; Hursthouse, M. B.; Malik, K. M. A. *Organometallics* **1994**, *13*, 2235–2243.
- (35) The stabilisation energy is estimated according to the following procedure: Full relaxation of the alkane ligand provides $E(A)$. The virtual energy of free DC1 is obtained from $E(\text{DC1}^*) = E(\text{DC1}) - E(A)$. In this case, it was found to be essentially similar to a single point energy calculated on DC1 with the alkane ligand removed. The final stabilization of DC1 relative to DC2 is formally obtained from $\Delta E = E(\text{DC1}^*) - E(\text{DC2})$, or explicitly $\Delta E = E(\text{DC1}) - E(\text{DC2}) - E(A)$.
- (36) Möller, A. C. Diplomarbeit, Universität Hamburg, Germany, 2001.
- (37) Frisch, M. J.; Trucks, G. W.; Schlegel, H. B.; Scuseria, G. E.; Robb, M. A.; Cheeseman, J. R.; Montgomery, J. A., Jr.; Vreven, T.; Kudin, K. N.; Burant, J. C.; Millam, J. M.; Iyengar, S. S.; Tomasi, J.; Barone, V.; Mennucci, B.; Cossi, M.; Scalmani, G.; Rega, N.; Petersson, G. A.; Nakatsuji, H.; Hada, M.; Ehara, M.; Toyota, K.; Fukuda, R.; Hasegawa, J.; Ishida, M.; Nakajima, T.; Honda, Y.; Kitao, O.; Nakai, N.; Klene, M.; Li, X.; Knox, J. E.; Hratchian, H. P.; Cross, J. B.; Adamo, C.; Jaramillo, J.; Gomperts, R.; Stratmann, R. E.; Yazyev, O.; Austin, A. J.; Cammi, R.; Pomelli, C.; Ochterski, J. W.; Ayala, P. Y.; Morokuma, K.; Voth, G. A.; Salvador, P.; Dannenberg, J. J.; Zakrzewski, V. G.; Dapprich, S.; Daniels, A. D.; Strain, M. C.; Farkas, O.; Malick, D. K.; Rabuck, A. D.; Raghavachari, K.; Foresman, J. B.; Ortiz, J. V.; Cui, Q.; Baboul, A. G.; Clifford, S.; Cioslowski, J.; Stefanov, B. B.; Liu, G.; Liashenko, A.; Piskorz, P.; Komaromi, I.; Martin, R. L.; Fox, D. J.; Keith, T.; Al-Laham, M. A.; Peng, C. Y.; Nanayakkara, A.; Challacombe, M.; Gill, P. M. W.; Johnson, B.; Chen, W.; Wong, M. W.; Gonzalez, C.; Pople, J. A. *Gaussian 03*, revision B.04; Gaussian, Inc.: Pittsburgh, PA, 2003.
- (38) (a) Becke, A. D.; *J. Chem. Phys.* **1993**, *98*, 5648. (b) Lee, C.; Yang, W.; Parr, R. G. *Phys. Rev. B* **1988**, *37*, 785.
- (39) Hay, P. J.; Wadt, W. R. *J. Chem. Phys.* **1985**, *82*, 270.
- (40) (a) Dunlap, B. I. *J. Chem. Phys.* **1983**, *78*, 3140. (b) Dunlap, B. I. *J. Mol. Struct. (Theochem)* **2000**, *529*, 37.
- (41) Flükiger, P.; Lüthi, H. P.; Portmann, S.; Weber, J. MOLEKEL 4.0; Swiss Center for Scientific Computing: Manno, Switzerland, 2000.